The Astrophysical Journal, 862:16 (19pp), 2018 July 20 https://doi.org/10.3847/1538-4357/aac9b9

The MAVERIC Survey: Still No Evidence for Accreting Intermediate-mass Black Holes in Globular Clusters

Evangelia Tremou[1], Jay Strader[1], Laura Chomiuk[1], Laura Shishkovsky[1], Thomas J. Maccarone[2], James C. A. Miller-Jones[3], Vlad Tudor[3], Craig O. Heinke[4], Gregory R. Sivakoff[4], Anil C. Seth[5], and Eva Noyola[6]
[1] Center for Data Intensive and Time Domain Astronomy, Department of Physics and Astronomy, Michigan State University, East Lansing, MI 48824, USA; tremou@msu.edu
[2] Department of Physics and Astronomy, Texas Tech University, Box 41051, Lubbock, TX 79409-1051, USA
[3] International Centre for Radio Astronomy Research, Curtin University, GPO Box U1987, Perth, WA 6845, Australia
[4] Department of Physics, University of Alberta, CCIS 4-181, Edmonton, AB T6G 2E1, Canada
[5] Department of Physics and Astronomy, University of Utah, Salt Lake City, UT, USA
[6] McDonald Observatory, University of Texas at Austin, Austin, TX 78712, USA
Received 2018 February 28; revised 2018 May 11; accepted 2018 May 30; published 2018 July 18

Abstract

We present the results of an ultradeep, comprehensive radio continuum survey for the accretion signatures of intermediate-mass black holes (IMBHs) in globular clusters (GCs). The sample, imaged with the Karl G. Jansky Very Large Array and the Australia Telescope Compact Array, comprises 50 Galactic GCs. No compelling evidence for an IMBH is found in any cluster in our sample. In order to achieve the highest sensitivity to low-level emission, we also present the results of an overall stack of our sample as well as various subsamples, also finding nondetections. These results strengthen the idea that IMBHs with masses $\gtrsim 1000 M_{\odot}$ are rare or absent in GCs.

Key words: black hole physics – globular clusters: general – radio continuum: general

1. Introduction

Intermediate-mass black holes (IMBHs) have been proposed as a population of black holes (BHs) with masses between those of supermassive BHs that reside at the centers of galaxies (typically $\gtrsim 10^6 M_{\odot}$) and those of stellar-mass BHs created through the deaths of massive stars ($\lesssim 100 M_{\odot}$). IMBHs (10^2–$10^5 M_{\odot}$; e.g., Noyola & Gebhardt 2006; Feng & Soria 2011) draw ongoing interest as promising seeds for the growth of supermassive BHs (Volonteri & Perna 2005). Many possible origins for IMBHs have been suggested, including the collapse of metal-free Population III stars (Madau & Rees 2001) or direct collapse from gas in low-mass halos (Loeb & Rasio 1994; Eisenstein & Loeb 1995; Bromm & Loeb 2003; Lodato & Natarajan 2006). Massive young star clusters have also been suggested as important IMBH formation sites, perhaps via runaway stellar mergers (Portegies Zwart & McMillan 2002; Gürkan et al. 2004; Portegies Zwart et al. 2004; Vanbeveren et al. 2009). Vesperini et al. (2010) suggested that a central BH can grow through the accretion of gas lost in these star clusters. Another potential channel for forming IMBHs is via sequential mergers of stellar-mass BHs in globular clusters (GCs; Miller & Hamilton 2002). These possibilities make GCs primary targets for the search for IMBHs.

Efforts to investigate the presence of IMBHs in GCs, and subsequently constrain their masses, utilize two main approaches: dynamical or accretion signatures. Stars residing near the cluster center, inside the putative sphere of influence of any IMBH, have been studied using kinematic measurements such as radial velocities and proper motions (Newell et al. 1976; Gebhardt et al. 2005; McLaughlin et al. 2006; Anderson & van der Marel 2010; Noyola 2010; Kamann et al. 2014). Compared to dynamical measurements of supermassive BHs in galaxy centers, these IMBH studies are much more challenging owing to the relatively low BH masses: there are few stars within the IMBH sphere of influence and, especially for low-mass IMBHs, the signature of a central point mass can be confused with a concentrated population of stellar remnants (den Brok et al. 2014). A more recent approach is to constrain the potential using precise timing of one or more radio pulsars (Freire et al. 2017; Kızıltan et al. 2017; Perera et al. 2017). Overall, despite claims of dynamical evidence for IMBHs in many individual Galactic GCs (e.g., Ibata et al. 2009; Noyola 2010; Lützgendorf et al. 2011; Feldmeier et al. 2013; Lützgendorf et al. 2013a), there is no consensus about the presence of an IMBH in any particular object.

An alternative approach, again drawing a parallel to studies of supermassive BHs, is to search for accretion evidence for IMBHs. The source HLX-1, located in the halo of galaxy ESO 243-49 at distance of 95 Mpc, offers the best current such case. X-ray, optical, and radio data suggest the likely presence of a $\sim 10^4$–$10^5 M_{\odot}$ IMBH accreting at close to the Eddington rate (Webb et al. 2012), possibly located at the center of a tidally stripped young nuclear star cluster (Farrell et al. 2014; Musaeva et al. 2015; Soria et al. 2017; Webb et al. 2017).

By contrast, any so-far undiscovered IMBHs in Galactic clusters would necessarily be in quiescence, accreting at an extremely low rate, akin to Sgr A*. They would therefore be best observed as radio continuum sources due to synchrotron emission from relativistic jets (Maccarone 2004; Maccarone et al. 2005; Maccarone & Servillat 2008), though in a few nearby clusters with very deep X-ray data these observations can offer comparable or better constraints on accretion than radio data (e.g., Haggard et al. 2013).

The radio methodology has been applied to deep radio imaging of the Galactic GCs M15, M19, and M22 by Strader et al. (2012) to set 3σ upper limits of $<1000 M_{\odot}$ on the masses of IMBHs in these clusters and has been extended by Wrobel et al. (2015, 2016) to extragalactic GCs in M81 and NGC 1023 (where nondetections were also found, at higher mass limits than for Galactic clusters) using a stacking analysis.

In this paper, we use deep radio observations from the Karl G. Jansky Very Large Array (VLA) and the Australia

Telescope Compact Array (ATCA) to search for accretion signatures of IMBHs in 50 Galactic GCs, using data obtained as part of the MAVERIC (Milky Way ATCA and VLA Exploration of Radio-sources in Clusters) survey. Our paper is organized as follows: in Section 2, we present the sample of GCs and the radio observations. Section 3 describes our methodology for determining IMBH mass constraints. In Section 4, we present the results for each cluster and the stack of all 50 Milky Way GCs. In Section 5 we discuss and analyze these results. An Appendix considers in detail the radio data for NGC 6624, which has a number of bright known radio sources near its center and a recent IMBH claim (Perera et al. 2017).

2. Radio Data and Reduction

2.1. Target Selection

The MAVERIC sample was chosen primarily by distance and mass and was intended to be complete for GCs with masses $>10^5\,M_\odot$ and distances <9 kpc, keeping in mind that many GCs near the bulge have uncertain distances. Massive clusters ($\gtrsim 5\times10^5\,M_\odot$) at larger distances were added to search for IMBHs. Objects at declinations $\delta > -35^\circ$ were primarily observed with the VLA and more southerly sources were observed with ATCA, though this division is not precise and a few clusters were observed with both arrays.

Here, we use the most recent updated distance measurements to sample GCs; distances and references are listed in Tables 1 and 2.

More details on the sample selection, observing setup, and source catalogs will follow in separate survey papers (L. Shishkovsky et al., in preparation; V. Tudor et al., in preparation).

2.2. VLA

VLA observations took place during 2011 May–August (NRAO/VLA Program IDs 10C-109 and 11A-269), 2012 September (12B-073) 2014 February–June (13B-014), and 2015 May–August (15A-100 and 15A-225). Data for 18 GCs were obtained in the most extended A configuration, with 7 more southerly clusters observed in the BnA configuration. The remainder of the GCs were observed during "move time" in or out of A configuration. With these extended configurations, we obtained angular resolutions $\lesssim 1''$ for nearly all VLA GCs, which facilitates the comparison between radio images and the optical centers. The median synthesized beam in the 5 GHz VLA image (and in the averaged 6 GHz images) is $0\farcs7\times0\farcs4$.

VLA observations were made with C band receivers (4–8 GHz). Data taken from 2011 to 2014 used 8 bit mode, with two independent 1024 MHz–wide basebands centered at 5.0 and 6.75 GHz. In 2015, we used 3 bit mode, with two independent 2048 MHz–wide basebands centered at 5.0 and 7.0 GHz. The amount of usable continuum for the 3 bit observations was less than double that in the 8 bit observations owing to significant radio frequency interference (RFI) in the band. In both modes the bandwidth was divided into 128 MHz–wide spectral windows, and each spectral window was sampled by 64 channels. All observations were obtained in full polarization mode.

We were approved to obtain 10 hr of observations per VLA cluster, which nominally would result in 7–8 hr on source, depending on the length of the individual observing blocks. The median on-source observing time was consistent with this goal, at 7.4 hr. Not all the requested blocks were successfully observed, and three clusters had final on-source times that were less than 5 hr (M54, Liller 1, and NGC 6522), with correspondingly higher rms noise levels. Observations typically alternated between 10 minutes on source and short observations of a phase calibrator (selected to be within 10 degrees of the science target). A bandpass and flux calibrator were observed at the start or end of each block.

Standard procedures were followed for data flagging, calibration, and imaging with the Common Astronomy Software Application package (CASA; McMullin et al. 2007) and the Astronomical Image Processing System (AIPS; Greisen 2003). Imaging of the data was carried out using a Briggs weighting scheme (robust = 1). To mitigate artifacts from large fractional bandwidth, the *uv* data were divided into two frequency chunks (basebands) and imaged separately. In CASA, frequency-dependent clean components (with two Taylor terms; `nterms = 2`) were also used in imaging to mitigate large-bandwidth effects (Rau 2012). For the GCs with bright sources that generated considerable artifacts, we applied self-calibration to optimize the image quality.

Of the 29 GCs with VLA data, 17 were taken primarily or only in 3 bit mode, which had 3–3.4 GHz of bandwidth remaining after RFI flagging. The median rms noise in each of the baseband images centered at 5.0 and 7.0 GHz was 2.0 μJy bm^{-1}. For nine GCs observed earlier in the project, the data were taken in 8 bit mode, which typically results in a 1.8 GHz bandwidth after flagging. Given the lower bandwidth, the baseband rms noise values were slightly higher, 2.5 μJy bm^{-1} (5.0 GHz) and 2.1 μJy bm^{-1} (6.75 GHz). The three GCs with comparable exposure times in 3 bit and 8 bit mode had noise levels intermediate between the 3 bit and 8 bit median values, as expected.

Given the expected flat spectrum of the radio continuum emission from low-luminosity accreting IMBHs, we also combined the individual basebands into a single image to maximize sensitivity. To do this, the higher-frequency image was convolved to the resolution of the lower-frequency image using the AIPS task `CONVL`. The high- and low-frequency images were then averaged using the AIPS task `COMB`, weighting by the variance. The median rms noise at 6.0 GHz is 1.5 μJy bm^{-1} (3 bit data) and 1.7 μJy bm^{-1} (8 bit data). The distribution of the observed image noise in the frequency averaged images is presented for all GCs in Figure 1.

2.3. ATCA

27 GCs were observed with ATCA (project code: C2877) in the extended 6A or 6D configurations in runs from 2013 to 2015. Archival data for 47 Tuc and ω Cen from Lu & Kong (2011) are also included in our analysis, imaged together with our newer data for these clusters. All observations were carried out using the Compact Array Broadband Backend (Wilson et al. 2011), allowing simultaneous observations in two bands centered at 5.5 and 9.0 GHz, each with 2 GHz of bandwidth. Observations were typically made over two to three separate blocks on different days. In each epoch, the target cluster and phase calibrator were alternately observed for 10–20 minutes and 1.5–2 minute integration times respectively, depending on atmospheric stability and calibrator brightness.

Flagging and calibration were performed in MIRIAD (Sault et al. 1995), and imaging was performed in CASA. As with the

Table 1
Results from VLA Data

ID	R.A. (J2000) (h:m:s)	Decl. (J2000) (° ′ ″)	Uncertainty (″)	Position Reference	Distance (kpc)	Distance Reference	3σ Flux Density (μJy)	3σ L_R (erg s^{-1})	IMBH Mass ($M_\odot$)	3σ L_X (erg s^{-1})	IMBH Mass Fraction	Core Radius (″)	Brownian Radius (″)
M3[a]	13 42 11.38	28 22 39.1	1.0	2	10.1	4	<5.8	$<3.5 \times 10^{27}$	<1460	$<7.8 \times 10^{30}$	<0.37	22.2	0.28
M5	15 18 33.21	02 04 51.8	0.2	2	7.7	1	<4.2	$<1.5 \times 10^{27}$	<1060	$<3.0 \times 10^{30}$	<0.28	26.4	0.38
M4	16 23 35.03	−26 31 33.8	1.0	2	1.8	30	<5.3	$<1.0 \times 10^{26}$	<390	$<1.5 \times 10^{29}$	<0.40	69.6	1.65
M107	16 32 31.86	−13 03 13.6	0.1	1	6.1	4	<5.6	$<1.3 \times 10^{27}$	<990	$<2.4 \times 10^{30}$	<1.14	33.6	0.50
M13	16 41 41.21	36 27 35.6	0.4	2	7.6	4	<4.9	$<1.7 \times 10^{27}$	<1110	$<3.4 \times 10^{30}$	<0.24	37.2	0.52
M12	16 47 14.18	−01 56 54.7	0.8	1	5.2	4	<4.3	$<7.0 \times 10^{26}$	<800	$<1.3 \times 10^{30}$	<0.92	47.4	0.78
M10	16 57 8.92	−04 05 58.0	1.0	13	4.4	6	<4.9	$<5.7 \times 10^{26}$	<740	$<1.0 \times 10^{30}$	<0.40	46.2	0.80
M62	17 01 12.98	−30 06 49.0	0.2	2	6.7	29	<6.6	$<1.8 \times 10^{27}$	<1130	$<3.6 \times 10^{30}$	<0.16	13.2	0.18
M19	17 02 37.80	−26 16 04.7	1.1	5	8.2	5	<4.8	$<1.9 \times 10^{27}$	<1170	$<4.0 \times 10^{30}$	<0.17	25.8	0.35
N6304	17 14 32.25	−29 27 43.3	0.2	1	5.9	7	<5.8	$<1.2 \times 10^{27}$	<980	$<2.3 \times 10^{30}$	<0.35	12.6	0.18
M92	17 17 07.43	43 08 09.26	0.1	2	8.9	1	<3.6	$<1.7 \times 10^{27}$	<1110	$<3.4 \times 10^{30}$	<0.41	15.6	0.22
N6325[b]	17 17 59.21	−23 45 57.6	2.0	6	6.5	8	<4.5	$<1.1 \times 10^{27}$	<960	$<2.2 \times 10^{30}$	<0.92	1.8	0.03
M9	17 19 11.78	−18 30 58.5	2.0	10	7.8	10	<3.8	$<1.4 \times 10^{27}$	<1030	$<2.7 \times 10^{30}$	<0.40	27.0	0.40
Liller 1	17 33 24.56	−33 23 22.4	0.3	3	8.1	12	<6.8	$<2.7 \times 10^{27}$	<1320	$<5.8 \times 10^{30}$	<0.20	5.4	0.07
M14	17 37 36.10	−03 14 45.3	0.5	6	9.3	6	<3.9	$<2.0 \times 10^{27}$	<1190	$<4.2 \times 10^{30}$	<0.15	47.4	0.64
Terzan 5	17 48 04.85	−24 46 44.6	1.0	11	5.9	19	<9.8	$<2.0 \times 10^{27}$	<1190	$<4.2 \times 10^{30}$	<0.21	9.6	0.13
N6440	17 48 52.70	−20 21 36.9	1.1	5	8.5	20	<6.5	$<2.8 \times 10^{27}$	<1340	$<6.1 \times 10^{30}$	<0.30	8.4	0.11
N6522[b]	18 03 34.89	−30 02 03.2	∼2[c]		7.7	6	<9.5	$<3.4 \times 10^{27}$	<1430	$<7.4 \times 10^{30}$	<0.36	3.0	0.04
N6539	18 04 49.68	−07 35 09.1	0.32	6	7.8	20	<4.4	$<1.6 \times 10^{27}$	<1090	$<3.2 \times 10^{30}$	<1.22	22.8	0.32
N6544	18 07 20.12	−24 59 53.6	0.95	8	3.0	20	<5.3	$<2.9 \times 10^{26}$	<570	$<4.7 \times 10^{29}$	<0.90	3.0	0.06
M28	18 24 32.73	−24 52 13.0	0.7	2	5.5	20	<5.1	$<9.2 \times 10^{26}$	<890	$<1.8 \times 10^{30}$	<0.24	14.4	0.23
M22	18 36 23.94	−23 54 17.1	0.8	1	3.1	28	<5.0	$<2.9 \times 10^{26}$	<570	$<4.7 \times 10^{29}$	<0.14	79.8	1.56
N6712	18 53 04.30	−08 42 22.0	0.5	9	8.0	9	<4.8	$<1.8 \times 10^{27}$	<1150	$<3.8 \times 10^{30}$	<0.90	45.6	0.63
M54	18 55 03.33	−30 28 47.5	0.1	1	23.9	15	<7.1	$<2.4 \times 10^{28}$	<2990	$<6.1 \times 10^{31}$	<0.21	5.4	0.04
N6760	19 11 12.01	01 01 49.7	0.5	6	7.4	20	<4.5	$<1.5 \times 10^{27}$	<1060	$<3.0 \times 10^{30}$	<0.42	20.4	0.29
M55	19 39 59.71	−30 57 53.1	0.8	1	5.7	4	<5.1	$<1.0 \times 10^{27}$	<910	$<1.9 \times 10^{30}$	<0.48	108.0	1.67
M15[b]	21 29 58.33	12 10 01.2	0.2	1	10.3	1	<6.3	$<4.0 \times 10^{27}$	<1530	$<9.0 \times 10^{30}$	<0.34	8.4	0.10
M2	21 33 26.96	−00 49 22.9	1.0	12	11.5	6	<3.9	$<3.1 \times 10^{27}$	<1390	$<6.8 \times 10^{30}$	<0.24	19.2	0.24
M30[b]	21 40 22.12	−23 10 47.5	0.1	1	8.6	4	<3.9	$<1.7 \times 10^{27}$	<1120	$<3.5 \times 10^{30}$	<0.84	3.6	0.05

Notes. We note that we assume 5 GHz as the central frequency in order to calculate the radio luminosities and the mass upper limits. The sources used for the photometric centers and the distances are shown at the bottom of the table. The core radius of Liller 1 is adopted from Saracino et al. (2015), while we use Harris (2010) for the rest of the clusters.

[a] GCs used for the stacking analysis are indicated in boldface.

[b] Core collapsed GCs as adapted by Trager et al. (1995) catalog.

[c] The center listed in the Harris (2010) catalog from Shawl & White (1986) is inconsistent with the apparent center of the cluster in the Two-Micron All-Sky Survey (2MASS). We redetermine the center using this 2MASS image, and this value is the one listed in Table 1. The uncertainty in the value is not well determined, but we estimate ∼2″.

References. (1) Goldsbury et al. (2010); (2) Miocchi et al. (2013); (3) Saracino et al. (2015); (4) Djorgovski (1987); (5) Picard & Johnston (1995); (6) Shawl & White (1986); (7) in't Zand et al. (2003); (8) Cohen et al. (2014); (9) Noyola & Gebhardt (2006); (10) Vanderbeke et al. (2015); (11) Lanzoni et al. (2010); (12) Dalessandro et al. (2009); (13) Dalessandro et al. (2011); (14) Cohen et al. (2007); (15) Watkins et al. (2015); (16) Watkins et al. (2016); (17) Baumgardt (2017); (18) Ferraro et al. (1999); (19) Valenti et al. (2007); (20) Harris (2010); (21) Valenti et al. (2005); (22) Ortolani et al. (2003); (23) Paltrinieri et al. (2001); (24) Arellano Ferro et al. (2013); (25) Ortolani et al. (2007); (26) Saracino et al. (2015); (27) Ortolani et al. (1999); (28) Kunder et al. (2013); (29) Contreras et al. (2010); (30) Kaluzny et al. (2013).

Table 2
Results from ATCA Data

ID	R.A. (J2000) (h:m:s)	Decl. (J2000) (° ′ ″)	Uncertainty (″)	Position Reference	Distance (kpc)	Distance Reference	3σ Flux Density (μJy)	3σ L_R (erg s^{-1})	IMBH Mass ($M_\odot$)	3σ L_X (erg s^{-1})	IMBH Mass Fraction	Core Radius (″)	Brownian Radius (″)
47 Tuc[a]	00 24 05.71	−72 04 52.2	0.5	2	4.6	15	<11.1	$<1.4 \times 10^{27}$	<1040	$<2.8 \times 10^{30}$	<0.13	21.6	0.32
N2808	09 12 03.10	−64 51 48.6	0.1	1	9.4	15	<8.8	$<4.7 \times 10^{27}$	<1620	$<1.0 \times 10^{31}$	<0.22	15.0	0.17
N3201	10 17 36.82	−46 24 44.9	1.0	1	4.9	18	<9.3	$<1.3 \times 10^{27}$	<1020	$<2.7 \times 10^{30}$	<0.68	78.0	1.15
N4372	12 25 45.40	−72 39 32.4	1.8	6	6.3	18	<9.9	$<2.4 \times 10^{27}$	<1250	$<4.9 \times 10^{30}$	<0.50	105.0	1.39
N4833	12 59 33.92	−70 52 35.4	0.3	1	6.7	18	<9.7	$<2.6 \times 10^{27}$	<1300	$<5.5 \times 10^{30}$	<0.53	60.0	0.77
ω Cen	13 26 47.28	−47 28 46.1	0.1	1	4.9	15	<8.8	$<1.3 \times 10^{27}$	<1000	$<2.5 \times 10^{30}$	<0.03	142.2	2.11
N5927	15 28 00.69	−50 40 22.9	0.2	1	7.9	15	<10.7	$<4.0 \times 10^{27}$	<1530	$<9.0 \times 10^{30}$	<0.43	25.2	0.30
N6139	16 27 40.37	−38 50 55.5	1.0	6	10.4	21	<10.8	$<7.0 \times 10^{27}$	<1880	$<1.6 \times 10^{31}$	<0.52	9.0	0.09
N6352	17 25 29.11	−48 25 19.8	0.6	1	5.6	20	<8.9	$<1.7 \times 10^{27}$	<1110	$<3.4 \times 10^{30}$	<1.18	49.8	0.70
N6362	17 31 54.99	−67 02 54.0	0.5	1	7.6	20	<7.8	$<2.7 \times 10^{27}$	<1320	$<5.8 \times 10^{30}$	<0.90	67.8	0.87
Terzan 1[b]	17 35 47.20	−30 28 54.4	1.1	5	5.2	13	<11.7	$<1.9 \times 10^{27}$	<1160	$<3.9 \times 10^{30}$	<0.52	2.4	0.03
N6388	17 36 17.23	−44 44 07.8	0.3	1	10.9	15	<8.4	$<6.0 \times 10^{27}$	<1770	$<1.4 \times 10^{31}$	<0.17	7.2	0.07
N6397[b]	17 40 42.09	−53 40 27.6	0.3	1	2.3	15	<10.5	$<3.3 \times 10^{26}$	<610	$<5.7 \times 10^{29}$	<0.69	3.0	0.05
N6441	17 50 13.06	−37 03 05.2	0.2	1	13.4	19	<10.8	$<1.2 \times 10^{28}$	<2270	$<2.9 \times 10^{31}$	<0.18	7.8	0.07
Terzan 6[b]	17 50 46.85	−31 16 29.3	0.6	7	6.8	20	<12.6	$<3.5 \times 10^{27}$	<1450	$<7.7 \times 10^{30}$	<1.24	3.0	0.03
Djorg 2	18 01 49.1	−27 49 33.0	3.0	10	7.0	23	<10.6	$<3.1 \times 10^{27}$	<1390	$<6.8 \times 10^{30}$	<1.29	19.8	0.24
N6541	18 08 02.36	−43 42 53.6	0.1	1	7.5	20	<11.7	$<3.9 \times 10^{27}$	<1520	$<8.8 \times 10^{30}$	<0.55	10.8	0.13
N6553	18 09 17.59	−25 54 38.0	2.0	14	6.0	20	<10.3	$<2.2 \times 10^{27}$	<1230	$<4.7 \times 10^{30}$	<0.52	31.8	0.42
N6624[b]	18 23 40.51	−30 21 39.7	0.1	1	8.4	19	<9.9	$<4.2 \times 10^{27}$	<1550	$<9.4 \times 10^{30}$	<2.12	3.6	0.04
N6652	18 35 45.63	−32 59 26.6	0.1	1	10.0	20	<10.7	$<6.4 \times 10^{27}$	<1820	$<1.5 \times 10^{31}$	<2.30	6.0	0.06
N6752[b]	19 10 52.11	−59 59 04.4	0.1	1	4.0	15	<10.5	$<1.0 \times 10^{27}$	<920	$<1.9 \times 10^{30}$	<0.38	10.2	0.15

Notes. We note that we assume 5 GHz as the central frequency in order to calculate the radio luminosities and the mass upper limits. The sources used for the photometric centers and the distances are shown at the bottom of the table. The core radii are adopted from Harris (2010).

[a] GCs used for the stacking analysis are indicated in boldface.

[b] Core collapsed GCs as adapted by Trager et al. (1995) catalog.

References. (1) Goldsbury et al. (2010); (2) Miocchi et al. (2013); (3) Saracino et al. (2015); (4) Djorgovski (1987); (5) Picard & Johnston (1995); (6) Shawl & White (1986); (7) in't Zand et al. (2003); (8) Cohen et al. (2014); (9) Noyola & Gebhardt (2006); (10) Vanderbeke et al. (2015); (11) Lanzoni et al. (2010); (12) Dalessandro et al. (2009); (13) Dalessandro et al. (2011); (14) Cohen et al. (2007); (15) Watkins et al. (2015); (16) Watkins et al. (2016); (17) Baumgardt (2017); (18) Ferraro et al. (1999); (19) Valenti et al. (2007); (20) Harris (2010); (21) Zinn & Barnes (1998); (22) Bogdanov et al. (2016); (23) Valenti et al. (2010).

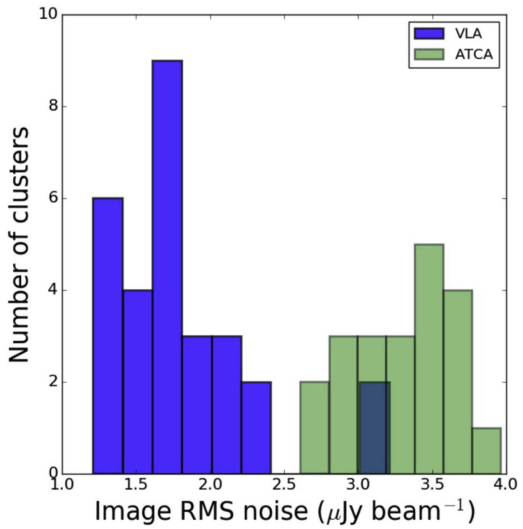

Figure 1. Distribution of the observed rms noise in our frequency-averaged images for 50 Galactic GCs. VLA data are blue and ATCA data are green.

VLA, the two frequency bands were imaged separately and with a Briggs robust value of 1. The median synthesized beam in the 5.5 GHz images (and in the frequency-averaged images) is $3\farcs2 \times 1\farcs6$. The median on-source integration time was 17.0 hr, yielding median rms noise levels of 4.1 and 4.6 μJy bm^{-1} in the 5.5 and 9.0 GHz bands, respectively. As with the VLA images, we averaged images in the two frequency bands together, and the median rms was 3.3 μJy bm^{-1} in the resulting 7.25 GHz images. This is about twice the median rms of the VLA images (Figure 2) but still very sensitive, allowing tight constraints on the presence of central radio sources. The distribution of the observed rms of the ATCA images (Figure 3) is shown in Figure 1.

Five GCs in the sample were observed by both VLA and ATCA; for all but NGC 6522 (which had only 2.5 hr on-source with the VLA) the beam size is smaller and the rms is substantially lower in the VLA images, so we use the VLA data for subsequent analysis.

2.4. Stacking Analysis

We also stacked all the clusters to give the highest sensitivity to low-level emission under the assumption that IMBHs exist in the centers of GCs. For the stack, we only used clusters that do not have any central radio emission (from unresolved pulsars or bright X-ray binaries), in order to make a weighted-mean image of these fields. In total, we used 24 clusters from VLA and 14 from ATCA observations, which are noted in boldface in Tables 1 and 2. Twelve clusters that were excluded from the deep stack are discussed extensively in Sections 3.3 and 4.2.

To do this, the frequency-averaged images were convolved to a common resolution ($2\farcs2$ for VLA data and $6\farcs0$ for ATCA data) using the AIPS tasks `CONVL`. Images were aligned so that the cluster centers aligned at the image center (see Tables 1 and 2 for GC centers). We then used the AIPS task `STACK` to produce the weighted mean image (see Lindroos et al. 2015 for details of the stacking technique). Separate stacks were made for VLA (Figure 4) and VLA (Figure 5) clusters (see Section 4.2).

3. Data Analysis

3.1. Linking IMBH Mass and Radio Luminosity

The "fundamental plane" of BHs describes the relation between X-ray luminosity ($L_{\rm X}$), radio luminosity ($L_{\rm R} = 4\,\pi\,d^2\,\nu\,S_\nu$), and the mass of the BH ($M_{\rm BH}$) for objects ranging from stellar-mass BHs to supermassive BHs (Merloni et al. 2003; Falcke et al. 2004; Plotkin et al. 2012). It implies that accreting BHs of all masses show a correlation between X-ray and radio luminosity but that more massive BHs have a higher ratio of $L_{\rm R}/L_{\rm X}$ at a fixed $L_{\rm X}$.

Since no IMBHs have been dynamically confirmed, their consistency with the fundamental plane has not been tested: their behavior is an interpolation between the extreme low and high BH masses. For this paper, we assume that accreting IMBHs would behave in a manner consistent with the fundamental plane, and we use our radio observations to constrain the masses of IMBHs at the centers of Galactic GCs.

We adopt the form of the fundamental plane with BH mass as the dependent variable (Miller-Jones et al. 2012; Plotkin et al. 2012):

$$\begin{aligned}\log M_{\rm BH} = {} & (1.638 \pm 0.070)\log L_{\rm R} \\ & - (1.136 \pm 0.077)\log L_{\rm X} \\ & - (6.863 \pm 0.790) \end{aligned} \quad (1)$$

where the black hole mass $M_{\rm BH}$ is given in units of $M_\odot$, and $L_{\rm X}$ and $L_{\rm R}$ are given in erg s^{-1}. This form of the fundamental plane is derived using BHs in the "low/hard" accretion state ($\lesssim$ a few percent of the Eddington rate), in which the X-ray emission is thought to originate in a corona or possibly near the base of the jet while the radio emission is partially self-absorbed synchrotron radiation from the jet. If IMBHs are present in GCs and accreting, then they must be in the low state or else they would be easily observed as bright X-ray sources. The respective luminosities in this plane are formally defined between 0.5–10 keV ($L_{\rm X}$) and at 5 GHz ($L_{\rm R}$). In all cases we assume flat radio spectra consistent with that observed for low-luminosity active galactic nuclei (AGNs), e.g: Nagar et al. (2000) (see also Blandford & Königl 1979; Hjellming & Johnston 1988; Gallo et al. 2005) to translate the observed flux density ($L_{\rm R}$) limits into 5 GHz luminosities.

Consistent with previous work, we assume that the putative IMBH accretes from ambient intracluster gas in a manner similar to low-luminosity central supermassive BHs in galaxies (Maccarone 2003; Pellegrini 2005; Strader et al. 2012; Haggard et al. 2013). In GCs, gas should be present due to the high density of red giants and their associated winds. Direct evidence of this gas has been seen in 47 Tuc and M15, revealed by the radial distribution of the dispersion measure of pulsars, which traces the free electron density inside the GC (Freire et al. 2001). These observations and the lack of H I in GCs implies that the gas must be mostly ionized (van Loon et al. 2006); here we assume that intracluster gas is evenly distributed and is fully ionized and isothermal at a temperature of $T = 10^4$ K. We assume a gas number density of $n = 0.2$ cm^{-3}, corresponding to an electron density of $n_e = 0.1$ cm^{-3}, consistent with the aforementioned pulsar data and expectations for freely expanding red giant winds (Pfahl & Rappaport 2001; Pooley & Rappaport 2006).

The Bondi accretion rate for an isothermal gas onto a BH is given by $\dot{M}_{\rm Bondi} = e^{3/2}\,\pi\,G^2\,M^2\,\rho\,c_s^{-3}$, where $e^{3/2} = 2(5-3\gamma)^{(5-3\gamma)/2(\gamma-1)}$, from $\gamma = 1$ for an isothermal gas;

G is the gravitational constant; M is the BH mass; and $\rho = n\ \mu\ m_H$ is the gas density (Bondi 1952). The sound speed c_s in an isothermal gas is given by $c_s = (k_B\ T/\mu m_H)^{1/2}$ for the mean molecular mass μ. Here we take $\mu = 0.59$, appropriate for ionized gas with the usual composition of a GC (Fall & Rees 1985). Substituting in typical values, the Bondi rate in units of g s^{-1} is

$$\dot{M}_{\rm Bondi} = 1.18 \times 10^{17} \left(\frac{M}{2000 M_\odot}\right)^2 \left(\frac{n}{0.2\ {\rm cm}^{-3}}\right) \left(\frac{T}{10^4\ {\rm K}}\right)^{-3/2}. \quad (2)$$

To yield the Bondi rate in units of $M_\odot$ yr^{-1}, the pre-factor on the above equation is instead 1.88×10^{-9}.

The results of Pellegrini (2005) show that low-luminosity AGNs are not as luminous as would be expected if they were accreting at the Bondi rate in a radiatively efficient manner (see also recent theoretical work on sub-Bondi accretion by Inayoshi et al. 2018). The quantity directly constrained by X-ray measurements is not the accretion rate itself but a combination of the radiative efficiency and the accretion rate. The X-ray luminosity is given by the standard equation $L_{\rm X} = \epsilon \dot{M} c^2$, for the radiative efficiency ϵ and the speed of light c. As in our previous work (Maccarone & Servillat 2008; Strader et al. 2012), we assume that the accretion flow is radiatively inefficient, as for example in an advection-dominated accretion flow (Narayan & Yi 1995), such that the radiative efficiency $\epsilon = \eta\ (\dot{M}/\dot{M}_{\rm edd})$ for some normalization η and $\dot{M}_{\rm edd}$ is the Eddington accretion rate.

If we parameterize the accretion rate $\dot{M}$ as a fraction f_b of the Bondi rate (so that $\dot{M} = f_b\ \dot{M}_{\rm Bondi}$), then the observationally determined quantity is ηf_b^2. Using the $\dot{M}_{\rm Bondi}$ and $L_{\rm X}$ measurements of Pellegrini (2005) for low-luminosity AGNs, and adjusting for their use of $\gamma = 4/3$ rather than our isothermal $\gamma = 1$, we find that the quantity ηf_b^2 has a median of about 0.005 but an extremely large spread of about 1.5 dex in the log. Considering its large uncertainty, this value is equivalent to the $\eta f_b^2 = 0.0045$ implicitly used in Strader et al. (2012), and for consistency we use this latter value. We discuss the uncertainty in this assumption and its implications for the mass limits below (Section 3.1.1).

Measuring the upper limits on the radio luminosity, $L_{\rm R}$, for a GC IMBH, we use the fundamental plane assuming that the BH follows the $L_{\rm R}$–$L_{\rm X}$ relationship and the accretion efficiency in order to determine the predicted $L_{\rm X}$ and subsequently to constrain the $M_{\rm BH}$. We emphasize that our methodology uses predicted $L_{\rm X}$ rather than observed $L_{\rm X}$ in the context of the fundamental plane to obtain IMBH mass constraints. This is because most GCs in our sample do not have published X-ray limits on a central IMBH. For one cluster (ω Cen) the published X-ray limit is more stringent than the limit inferred from our formalism (see Section 5.2.1). Given the scatter in the fundamental plane, additional observed X-ray limits would also provide valuable constraints on the presence of IMBHs in our GC sample, and our team is currently in the process of conducting a uniform X-ray analysis of the sample.

For the rest of this paper, we use 3σ upper limits as a constraint on the radio luminosity to constrain the IMBH mass. The plane between $M_{\rm BH}$ (in $M_\odot$), the distance d (in kpc), and the observed 5 GHz flux density or upper limit S (in μJy) implied by the above formalism is $\log M_{\rm BH} = 0.743 \log d + 0.372 \log S + 2.134$.

3.1.1. Uncertainties in This Formalism

As discussed in Strader et al. (2012), the main uncertainty in the mass limits predicted by this formalism is the combination of the radiative efficiency and the actual accretion rate, here parameterized by ηf_b^2. The scatter in the fundamental plane itself is nearly negligible. The observational scatter of about 1.5 dex in ηf_b^2 translates into a 0.39 dex scatter in $\log M_{\rm BH}$. Another source of uncertainty is the gas density ρ, but this is much harder to quantify given the scarcity of observational data. An uncertainty of 0.3 dex in $\log \rho$, suggested by the few Galactic GC data points as well as the theoretical considerations discussed above, barely increases the overall uncertainty in $\log M_{\rm BH}$ (to 0.43 dex). But we emphasize that the distribution of ρ is not well constrained.

A systematic uncertainty is our assumption of an isothermal gas rather than an adiabatic gas or one with an intermediate index. The isothermal assumption is conservative: it produces higher limits on $M_{\rm BH}$ than other choices. If we instead used the opposite extreme, then an adiabatic gas with $\gamma = 5/3$, $\log M_{\rm BH}$ would be lower by 0.52 dex. This is of the same order as the variation due to ηf_b^2, though the quantities are not necessarily independent.

The above discussion illustrates that the exact predictions depend on the assumptions made and that these limits should not be compared to other radiative limits on X-ray or radio emission without an appropriate consideration of the assumptions.

3.2. IMBH Location

We adopt the photometric center of each GC as the best current estimate of its center of mass. These are listed in Tables 1 and 2. The photometric centers come primarily, though not exclusively, from fitting models to *Hubble Space Telescope* (*HST*) star count observations. For example, Goldsbury et al. (2010) determined the photometric centers of 65 Milky Way GCs by performing an analysis of star counts in *HST*/Advanced Camera for Survey images, while Miocchi et al. (2013) supplemented *HST* observations with ground-based data.

Dynamical friction leads an IMBH to spiral to the center of mass of its host cluster on a short timescale (Matsubayashi et al. 2007). From this location, encounters with stars or stellar remnants can perturb the IMBH, especially if the BH mass is relatively low. Using the principle of Brownian motion, Chatterjee et al. (2002) analyzed the dynamics in the context of a BH at the center of a dense stellar cluster. Assuming a Plummer potential for the stellar system surrounding the central BH, the predicted variance of mean-squared one-dimensional deviations will be $\langle x^2 \rangle = (2/9)(M_*/M_{\rm BH}\ r_c^2)$, where M_* is the average mass of a star in the cluster core ($\sim 1 M_\odot$) and r_c is the cluster core radius (see also Strader et al. 2012). The core of a GC can be depleted of lower-mass stars due to mass segregation; therefore, we adopt a conservative value for the mass of the observable stars in the core of GCs (Fregeau et al. 2002). The actual motion of an IMBH would depend of course on the detailed mass profile of the inner regions, but this basic estimate gives a guide to how much the IMBH might wander as a function of cluster parameters. To calculate the Brownian radii for our GCs, we use the 3σ mass limits as given in Tables 1 and 2. For GCs with a cluster centroid uncertainty that

is larger than the Brownian radii, we use the former for our analysis.

We note that when the current paper was close to submission, de Vita et al. (2018) published a more sophisticated model, based on *N*-body simulations, for predicting the random motion of IMBHs in GC centers. Nonetheless, their results are generally consistent with the simple Brownian motion model we use.

3.3. Notes on Clusters with Radio Sources near Their Centers

Our basic result is that we find no compelling evidence for accreting IMBHs in any of the 50 GCs in our sample. However, some clusters do have radio sources near their photometric centers, which are associated with X-ray binaries or pulsars. Here we discuss these sources and why we favor non-IMBH explanations for the emission in all cases. Furthermore, previous studies regarding the IMBH existence in individual clusters are discussed extensively in Section 5.2.

3.3.1. Liller 1

This massive dense cluster shows several steep spectrum sources near the center (but outside the Brownian radius of a putative IMBH). Given the high interaction rate inferred for Liller 1 (Saracino et al. 2015) and the strong steep-spectrum emission as identified by Fruchter & Goss (2000), these sources are likely to be pulsars. Their presence does not affect the IMBH limits for the cluster, but we exclude it from the VLA stack.

3.3.2. M15

Our nondetection of an IMBH in M15 has previously been published in Strader et al. (2012). As discussed in that work, there are two previously known radio bright X-ray binaries and a pulsar near the cluster center (within 4″; Wolszczan et al. 1989; Johnston et al. 1991; Miller-Jones et al. 2011). However, there is no radio emission at the center of M15 within the Brownian radius expected for an IMBH. See Strader et al. (2012) for more discussion.

3.3.3. M62

M62 has six pulsars known in its core (D'Amico et al. 2001; Possenti et al. 2003; Lynch et al. 2012), two within 2.″5 of the cluster center. One of these, J1701−3006F, is a 4.5σ detection in our 4.7 GHz image but is not detected at 7.4 GHz. There is no significant detection at either frequency within the Brownian radius of an IMBH.

3.3.4. NGC 6388

NGC 6388 was previously observed with ATCA to search for an IMBH, and no central radio emission was detected to a level $<42\,\mu$Jy at 5.5 GHz (Bozzo et al. 2011).

In our ATCA 5.5 GHz image, there is a source located near the cluster center with the flux density $20.2 \pm 3.6\,\mu$Jy and a J2000 location of (R.A., decl.) = (17:36:17.276, −44:44:09.03), just 1.″1 from the cluster photometric center (Figure 3). The source is not significantly detected in the 9.0 GHz image, with a flux density at its location of $4.6 \pm 3.6\,\mu$Jy. If we conservatively assume a uniform prior on α between –3 and 3 and use the 3σ upper limit of the 9.0 GHz flux density ($<10.8\,\mu$Jy), then the most likely value of α is –2.1, with a 3σ upper limit to the spectral index of –0.2. Therefore the most probable interpretation is that this central source is a pulsar in the cluster, but a flat-spectrum source cannot be definitively ruled out.

The presence of a pulsar near the cluster center would be far from surprising, as a large pulsar population is expected in NGC 6388 based on the *Fermi*/LAT detection of GeV γ-rays (Abdo et al. 2010), its high stellar encounter rate (Bahramian et al. 2013), and its large X-ray source population (Bozzo et al. 2011; Maxwell et al. 2012). In addition, the centroid uncertainty for an IMBH of mass $>1000\,M_{\odot}$ in NGC 6388 is $\lesssim$0.″3. We therefore conclude that the central point source is not an IMBH but could be a pulsar. We proceed by using the 9.0 GHz image to constrain the mass of an IMBH; the limit listed in Table 2 corresponds to the sensitivity of the 9.0 GHz image alone.

3.3.5. NGC 6624

The center of the cluster NGC 6624 has two neutron star sources that emit in the radio: the bright pulsar PSR 1820-30A and the ultracompact low-mass X-ray binary 4U 1820-30 (Figure 6). Radio timing observations of the pulsar and X-ray timing of the X-ray binary have been used in a number of recent papers to argue for the presence of an IMBH (Peuten et al. 2014; Perera et al. 2017), though Gieles et al. (2018) argue that standard dynamical models of this GC can explain these observations without a massive BH.

Consistent with previous work, we observe a bright radio source near the center of NGC 6624 (Figure 6). Using these ATCA data and new *HST* observations, we find that all of the radio emission observed is consistent with being from the X-ray binary 4U 1820-30. We also note that this is in agreement with the Migliari et al. (2004) finding that 4U 1820-30 dominates above 2 GHz, and the pulsar below that. As the level of detail necessary to reach this conclusion is out of the main line of our paper, we place most of it in the Appendix and here focus only on the radio emission from an IMBH.

To search for residual emission from a possible IMBH, we subtracted the X-ray binary 4U 1820-30 from each of the 5.5 and 9.0 GHz images, assuming it was a point source. We fit a Gaussian component in the image–plane using the AIPS task `JMFIT` and then subtracted it, without any assumption on the spectral index value. No residuals are apparent in either image after the subtraction, suggesting that this assumption is reasonable. We remeasured the rms noise in a 24″ box around the cluster center after the subtraction, using this value for the IMBH limits. We find an rms noise of 4.2 μJy bm^{-1} at 5.5 GHz, 3.9 μJy bm^{-1} at 9.0 GHz, and 3.3 μJy bm^{-1} in the averaged image at 7.25 GHz. We use this latter limit to determine the IMBH mass limit using our standard formalism.

3.3.6. NGC 6652

NGC 6652 has a high central density, suggesting the efficient production of dynamically formed compact object binaries (Stacey et al. 2012), and several relatively bright X-ray sources have been detected by Chandra in this cluster. Only one radio pulsar has yet been detected in this cluster (DeCesar et al. 2015), but NGC 6652 is detected with *Fermi*/LAT at GeV energies, suggesting a substantial total population of millisecond pulsars (Abdo et al. 2010).

We detect a steep spectrum source in the ATCA image (present at 5.5 GHz and absent at 9.0 GHz) that is offset by

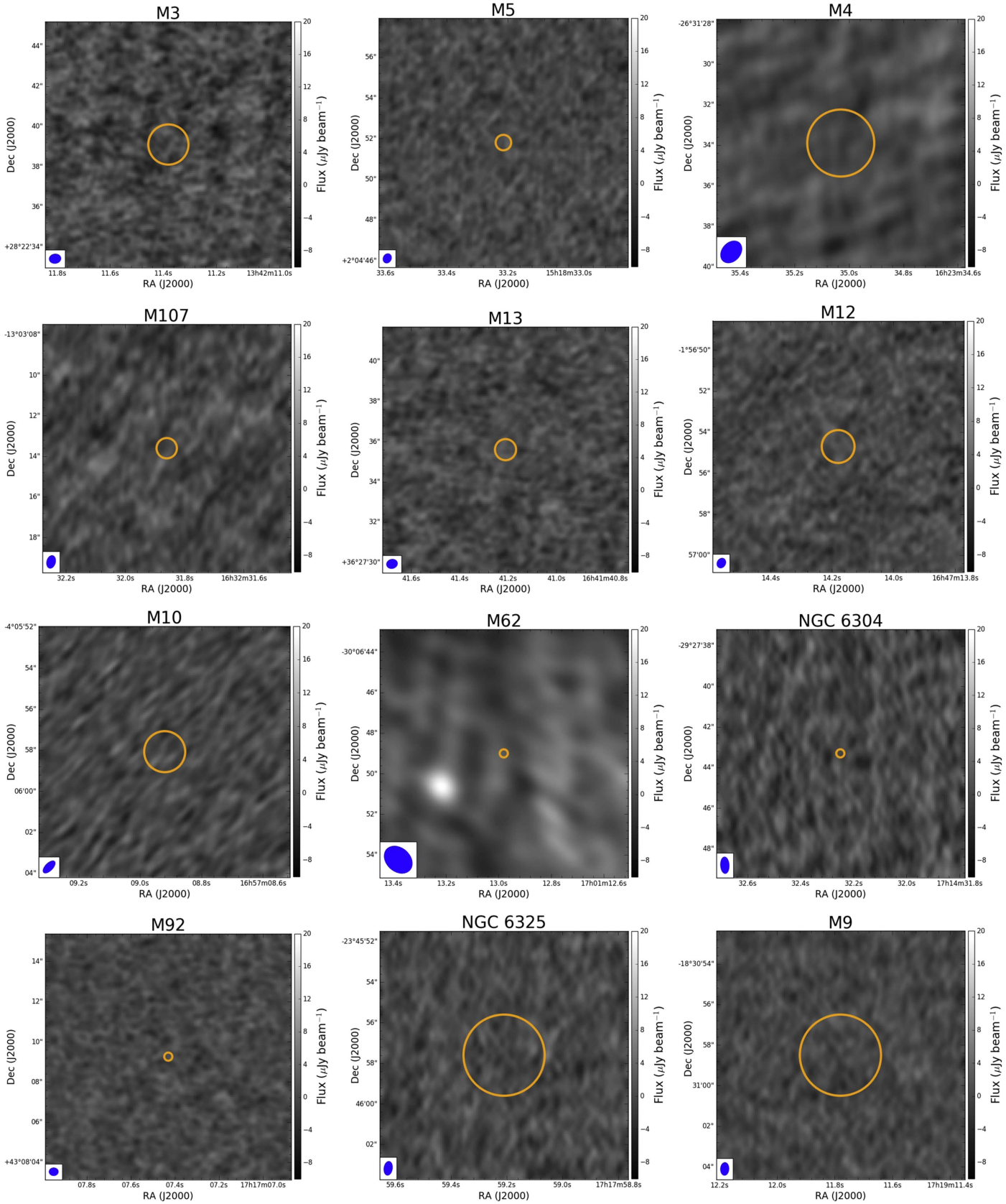

Figure 2. VLA frequency-averaged images of the GCs listed in Table 1, showing the central $12\farcs2 \times 12\farcs2$ for each cluster. The position of the cluster center is marked as an orange circle, and its size is matched to the wander radius of a putative IMBH. Synthesized beams are shown in blue in the bottom-left corner of all images.

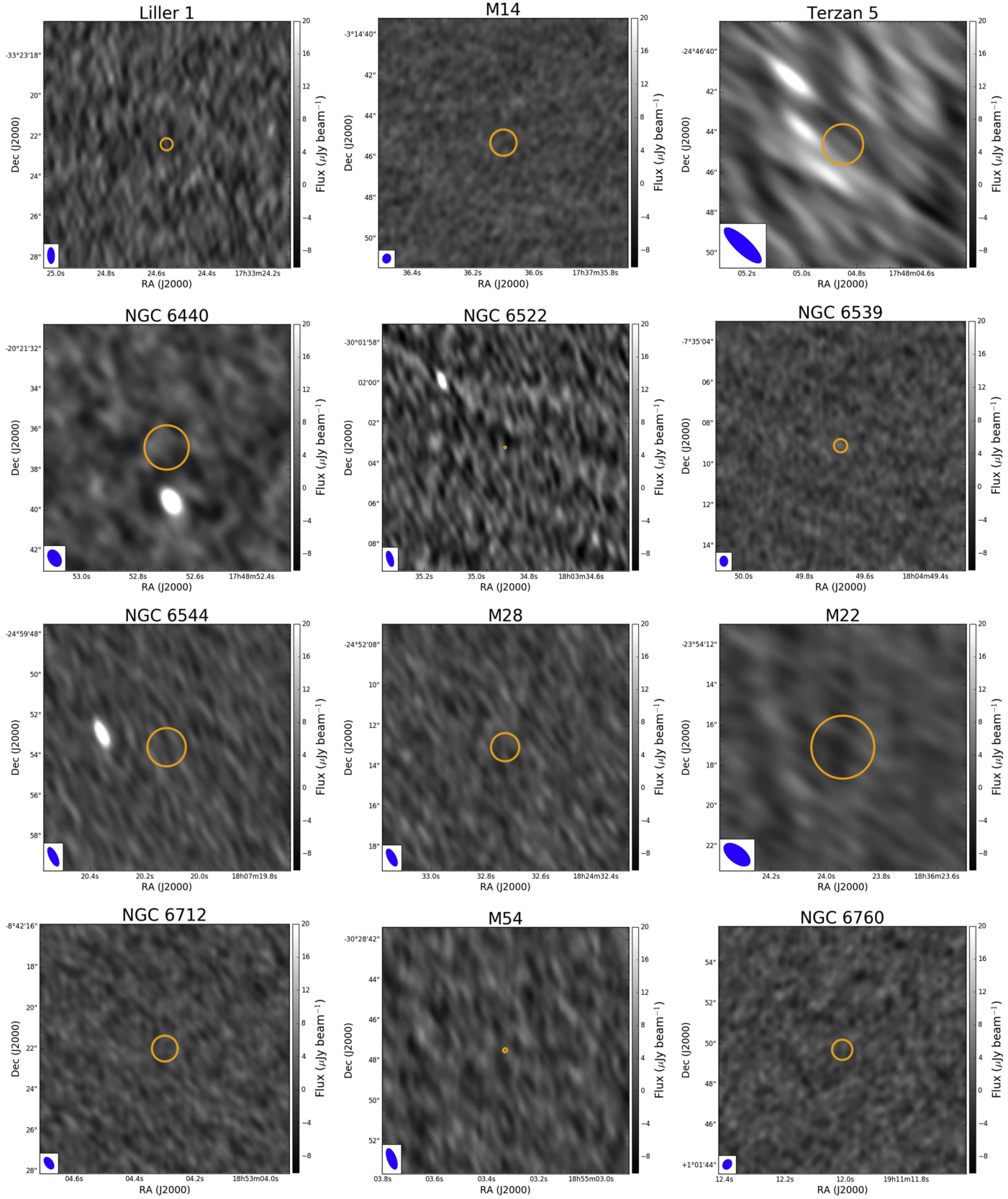

Figure 2. (Continued.)

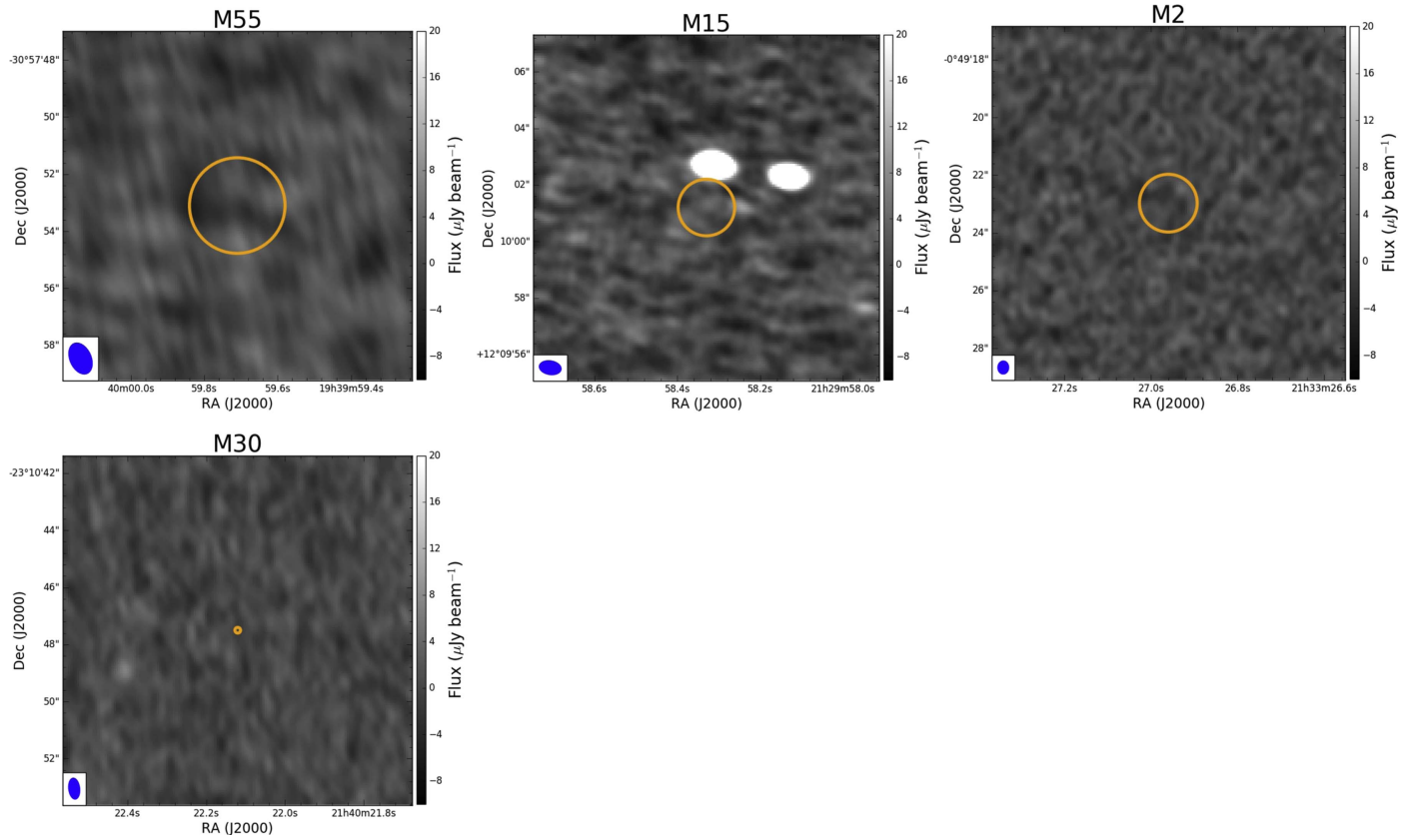

Figure 2. (Continued.)

about 1.″5 from the cluster center, so we can conclude that it is not associated with an IMBH. Just as for the central source in NGC 6388, the inferred steep spectrum implies that this source is likely a pulsar. This radio source is also 1.″5 from the nearest X-ray source in the cluster (source D of Stacey et al. 2012), ruling out an association. To place limits on the presence of an IMBH in NGC 6652, we only use the 9.0 GHz image, which does not show emission from this source.

3.3.7. Terzan 1

There is a radio source near the center of Terzan 1 with position J2000 (R.A., decl.) = (17:35:47.204, −30:28:54.89). This source may be associated with the quiescent X-ray binary CX2 (Cackett et al. 2006). However, we measure flux densities of 90.5 ± 4.1 μJy at 5.5 GHz and 34.5 ± 4.1 μJy at 9.0 GHz, implying a steep spectral index of $\alpha = -2.0 \pm 0.3$, more consistent with a pulsar than an X-ray binary. We will revisit this source in future work; in any case, the steep spectrum is inconsistent with the expectations for low-level accretion onto an IMBH.

To search for any residual emission that may be present from an IMBH, we subtracted this source from the 5.5 and 9.0 GHz images under the assumption that it is a point source, applying the same technique as in NGC 6624. No residuals are apparent in the 5.5 GHz image. In the 9.0 GHz image, a second source is visible at the $\sim 3\sigma$ level (in fact, this source is approximately one beam away from the brighter source in the original 9.0 GHz image and is clearly detectable there as well). This source is 3″ from the cluster center, far outside the Brownian radius of a $>1000 M_{\odot}$ IMBH, and hence cannot be attributed to an IMBH.

We re-estimate the rms noise from these residual images in a region 24″ wide centered on the cluster center. We find rms sensitivities of 4.8 μJy beam^{-1} at 5.5 GHz, 4.1 μJy beam^{-1} at 9.0 GHz, and 3.9 μJy beam^{-1} in the combined frequency image and use these revised values for our analysis.

3.3.8. Terzan 5

Terzan 5 hosts a large population of pulsars, with 38 known in the cluster core (Ransom et al. 2005; Prager et al. 2017; Cadelano et al. 2018, P. Freire's "Pulsars in Globular Clusters" page[7]), and our images show many point sources. However, assuming a 1″ uncertainty on the position of the cluster center and an IMBH Brownian radius of 0.″12, we find no VLA radio sources located right at the cluster center. ATCA images are also consistent with no flux at the cluster center but are less constraining because of the lower image resolution and poorer sensitivity.

3.3.9. Terzan 6

Terzan 6 hosts the known transient neutron star X-ray binary GRS 1747-312 near its center (at a projected distance of 0.″8; Predehl et al. 1991; Pavlinsky et al. 1994; in't Zand et al. 2003). This source was in outburst and radio bright during our observation (its X-ray/radio correlation will be reported elsewhere), measured at 21.4 ± 5.1 μJy in our ATCA 5.5 GHz image and 17.3 ± 5.3 μJy in the 9.0 GHz image. We

[7] http://www.naic.edu/~pfreire/GCpsr.html

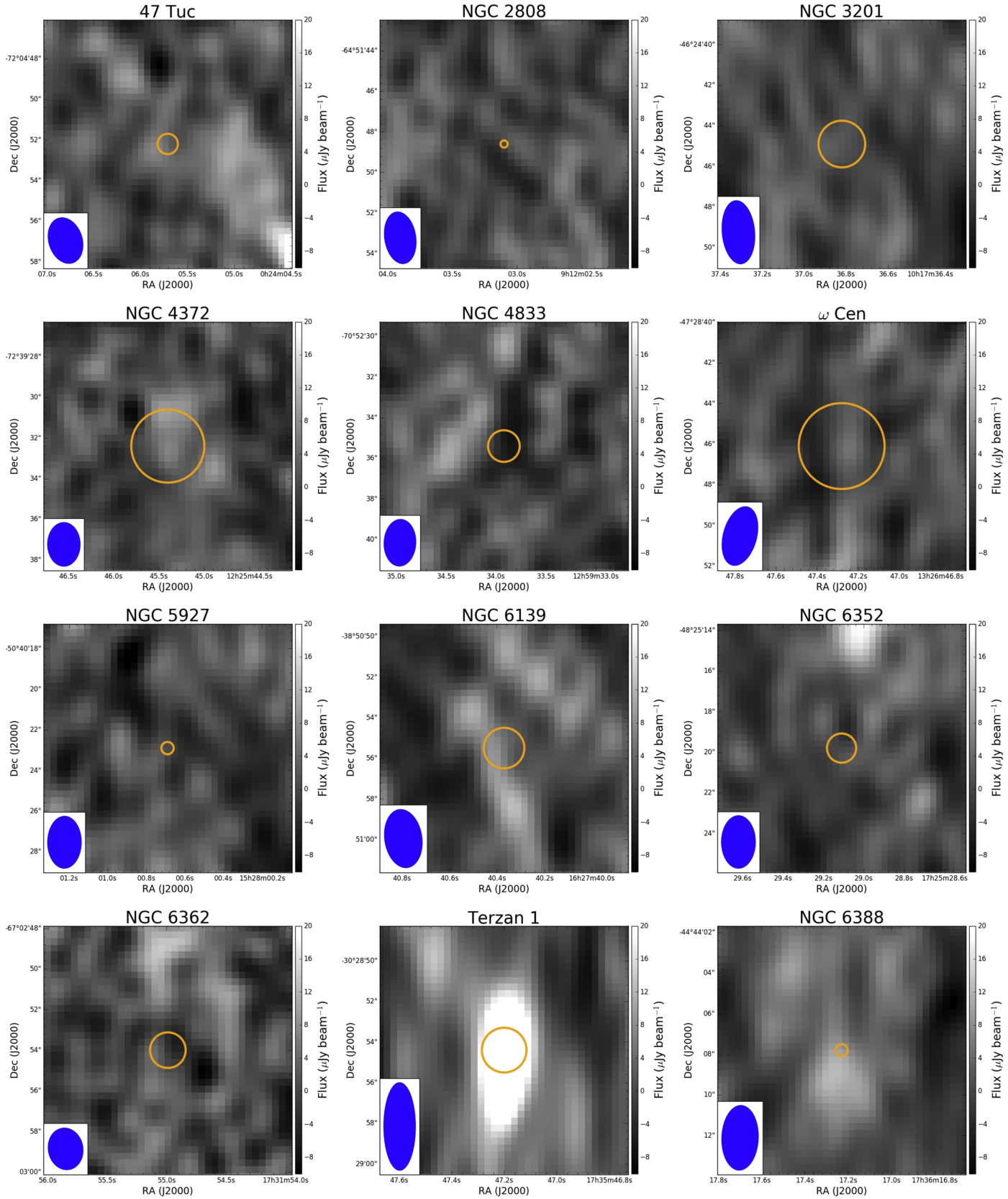

Figure 3. ATCA frequency-averaged images of the GCs listed in Table 2. See Figure 2 for more details.

subtracted this point source, and there is no residual emission near the cluster center. We remeasured the rms sensitivities of these residual images in a 24″ region and found 5.3 μJy beam^{-1} at 5.5 GHz, 5.3 μJy beam^{-1} at 9.0 GHz, and 4.2 μJy beam^{-1} in the frequency-averaged image, which we use for our IMBH limits.

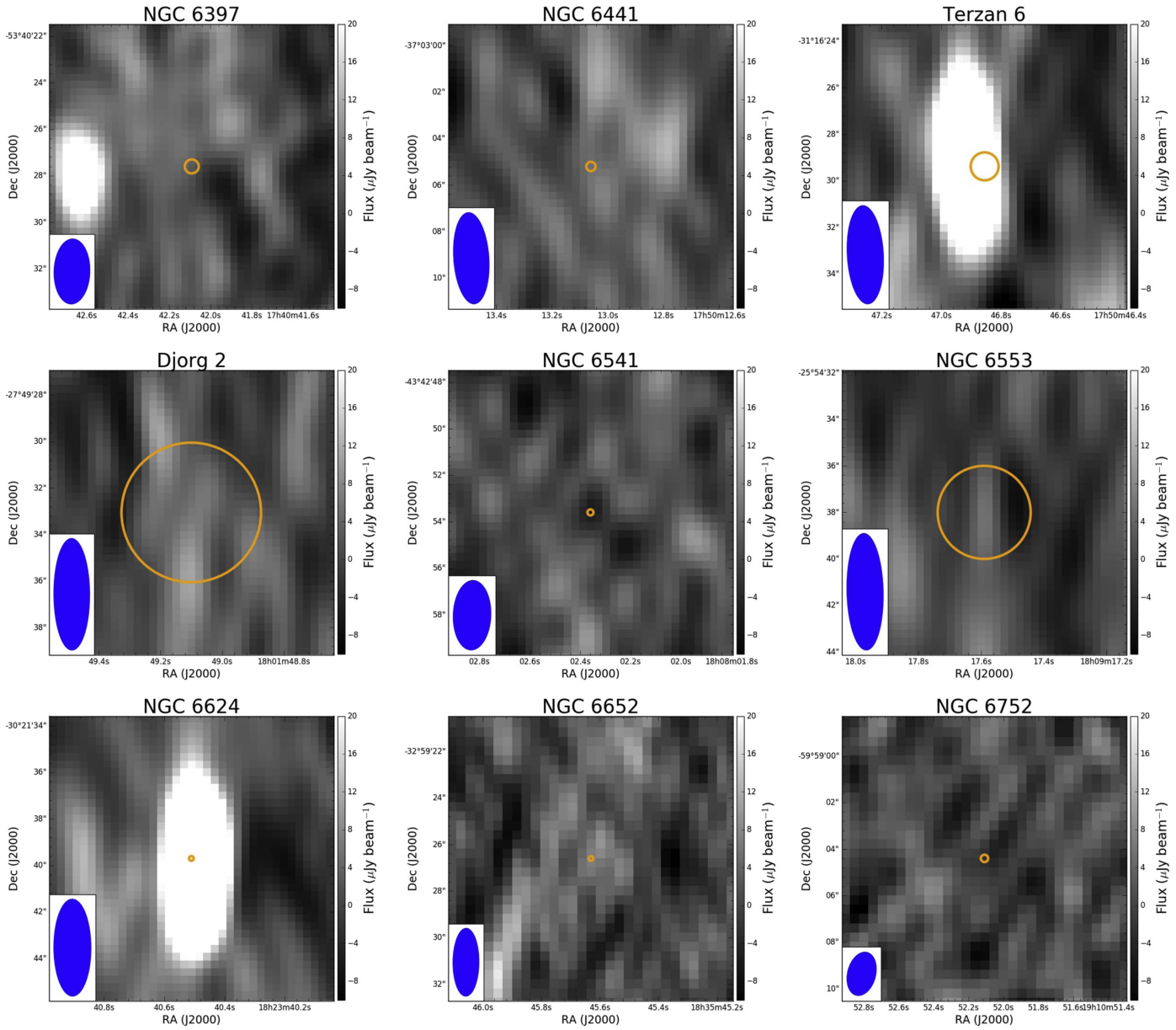

Figure 3. (Continued.)

4. Results

4.1. IMBH Mass Limits per Cluster

We followed the method described in Section 3.2 to search for IMBHs in cluster centers. The clusters discussed in Section 3.3 were considered individually, as detailed above, due to confusing sources near their centers.

For the rest of the targets, no radio emission was detected above 3σ that matches the photometric center within the cluster centroid uncertainty or Brownian radius. Figures 2 and 3 show the radio continuum images of these clusters, zoomed in on their centers.

The 3σ flux density upper limit was translated to an upper limit on luminosity assuming distances in Tables 1 and 2 and flat radio spectra. The median radio luminosity 3σ upper limit is $L_{\rm R} \lesssim 1.9 \times 10^{27}$ erg s^{-1}. We then use the formalism described in Section 3.1 to convert this luminosity upper limit to an IMBH mass upper limit. In Figure 7, we plot the IMBH mass upper limits as a function of radio flux density, with cluster distance included as the color scale. The most distant cluster is M54 at ∼24 kpc, which was excluded from the cluster stack owing to its much larger distance (Section 4.2).

Our median IMBH mass limits are $<1110 M_{\odot}$ (VLA clusters) and $<1320 M_{\odot}$ (ATCA clusters). Limits on individual clusters are listed in Tables 1 and 2, with the extreme limits of $<390 M_{\odot}$ and $<2990 M_{\odot}$ for the nearest and most distant clusters with VLA data: M4 and M54, respectively.

In these tables we also list the predicted 3σ X-ray luminosity limits corresponding to the IMBH mass limits and 3σ radio limits in the context of our formalism. The median predicted X-ray limits for the VLA and ATCA samples are $<3.4 \times 10^{30}$ and $<5.8 \times 10^{30}$ erg s^{-1}, respectively. For most clusters the radio limits on the presence of an IMBH are deeper than published X-ray limits, with the exception of ω Cen, which we discuss below in Section 5.2.1.

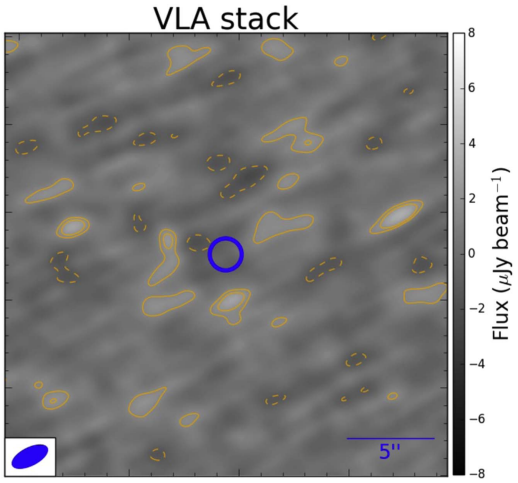

Figure 4. Weighted-mean stack of 24 clusters observed with VLA showing the central $25\farcs2 \times 25\farcs2$ area. The stacked image has an rms noise of 0.65 μJy beam^{-1}. The contours represent flux densities of -2σ (dotted), 2σ, and 3σ. The blue circle shows the mean IMBH wander radii ($0\farcs91$), and the radio beam is shown in the bottom left corner.

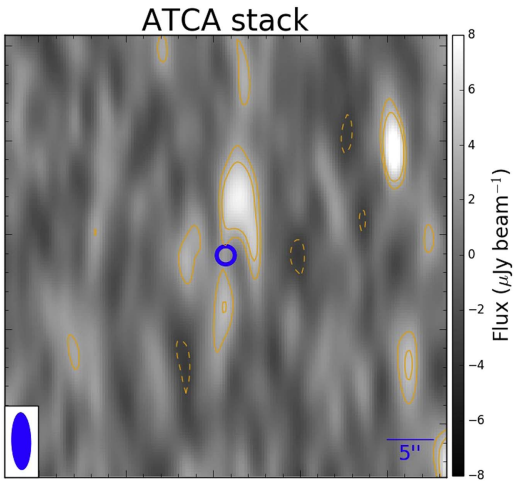

Figure 5. Weighted-mean stack of 14 clusters observed with ATCA showing the central $47\farcs8 \times 47\farcs8$ area. The stacked image has an rms noise of 1.42 μJy beam^{-1}. The contours represent flux densities of -2σ (dotted), 2σ, and 3σ. The blue circle shows the mean IMBH wander radii ($0\farcs96$), and the synthesized beam is shown in the bottom left corner.

These tables also list the 3σ IMBH mass limits expressed as a percentage of the total cluster mass. The GC masses are mostly from the recent work of Baumgardt & Hilker (2018), excepting four GCs not in that paper, for which we use the M_V listed in Harris (1996) and assume $M/L_V = 2$. For the VLA sample, the median 3σ IMBH mass limit is $<0.36\%$ of the cluster mass; for the ATCA sample, it is $<0.52\%$. We discuss these limits in the context of theoretical predictions in Section 5.3.

4.2. Deep Limits from Image Stacking

The analysis above reflects mass limits on accreting IMBHs in individual GCs. If we instead assume that the IMBH occupation fraction is high, then we can set deeper limits on the presence of such IMBHs by stacking the cluster images.

Section 2.4 describes our technique for co-adding the cluster images, resulting in the deep images presented in Figures 4 and 5. The distant GC M54 and GCs with stellar radio sources coinciding with their photometric centers (Section 3.3) were excluded from these stacks. We also excluded NGC 6139 because there is a 3.2σ flux peak $0\farcs6$ from the cluster center at 9.0 GHz. There is no emission at this location at 5.5 GHz, and the 9.0 GHz emission appears to be an artifact associated with a bright source $3\farcm4$ from the center. Djorg 2 does not have a central source but also shows artifacts associated with a bright source $2\farcm5$ from the center and is likewise excluded. Finally, NGC 4372 does not contain a significant central source but shows diffuse "fuzz" in the frequency-averaged image. NGC 4372 does not have a particularly large interaction rate (Bahramian et al. 2013), so it is not clear that a population of pulsars is expected; we defer a detailed comparison of interaction rates to radio source populations to a future work and for now exclude NGC 4372 from the ATCA stack.

For the VLA stack we included 24 clusters that have a median (mean) distance of 7.7 (6.9) kpc. The rms sensitivity of the co-added image is 0.65 μJy beam^{-1}, and there is no significant source detected at the center of the stacked image. Using our formalism, this corresponds to a 3σ VLA stack limit of $<800M_\odot$ ($<730M_\odot$). For this limit, the implied $L_X/L_{edd} \sim 10^{-11}$.

For the ATCA stacked image we averaged 14 clusters with a median (mean) distance of 6.8 (6.5) kpc. The image rms sensitivity is 1.42 μJy beam^{-1}, and no central source is detected. The corresponding 3σ ATCA stack limit is $<970M_\odot$.

Since many authors have argued that the densest ("core collapse") clusters are unlikely to contain IMBHs (e.g., Baumgardt et al. 2005; Trenti 2006; Noyola & Baumgardt 2011), we also created VLA and ATCA stacks excluding those GCs typically identified as core collapsed. Many of these were already excluded for individual reasons as we have noted. As expected, these new stacked images had slightly higher rms values than the full VLA and ATCA stacks (about 1.0 and 1.5 μJy beam^{-1}, respectively) and do not show significant central sources. Hence the exclusion of these GCs does not affect any of our conclusions.

5. Discussion and Conclusions

Our main result is that there is no accretion evidence for IMBHs with masses $\gtrsim 1000M_\odot$ in any Milky Way GC. We first discuss general uncertainties in our analysis and then specific cases of GCs where IMBHs have been claimed in previous work.

5.1. Uncertainties on Mass Limits

The logical basis for our constraints can be divided into three parts: if an IMBH is present, (1) is gas also present, (2) is this gas accreted by the IMBH, and (3) does this accreting gas produce the assumed radio signature?

That *some* gas is present in the core of GCs is certain—the winds of red giants supply an ongoing flux of material, and ionized gas has been observed in 47 Tuc, with some evidence in M15 (Freire et al. 2001). As 47 Tuc is rich in millisecond pulsars, this obviates the suggestion that such energy sources will reduce the plasma density to negligible amounts (Spergel 1991), though many mechanisms may well be responsible for clearing out much of the gas lost from stars (see, e.g., the discussion in Naiman et al. 2013). Additional

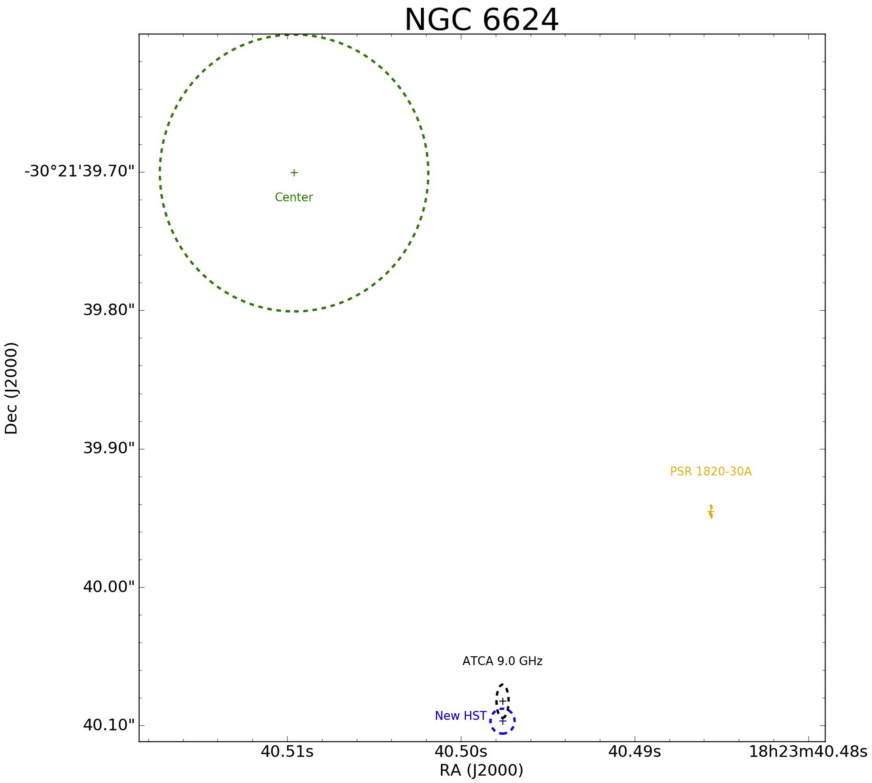

Figure 6. Central region of NGC 6624. The photometric center is marked with a green cross, and the position uncertainty is represented with the green dashed circle ($\sim 0\farcs1$ in radius). At radio wavelengths, the center of NGC 6624 is dominated by the well-known neutron star sources PSR 1820-30A and 4U 1820-30. The position of the optical counterpart to 4U 1820-30 is shown with the blue dashed circle; the radius denotes the uncertainty on the position. The position and uncertainty of the radio source in our ATCA images is shown as a black ellipse. The position of the PSR 1820-30A is marked in orange (Perera et al. 2017).

measurements of the ionized gas density in clusters and more sophisticated models of the intracluster medium are desirable.

Since no $\sim 1000 M_{\odot}$ IMBHs are known, all discussions of their properties necessarily involve indirect inferences. "Low-mass" central BHs with $\sim 10^5$–$10^6 M_{\odot}$ are present and are evidently accreting gas in the nuclear star clusters of nearby galaxies (Nguyen et al. 2017; Nyland et al. 2017), with even lower-mass BHs detected at higher accretion rates in more distant galaxies (Baldassare et al. 2015). At least in terms of their mass, these systems probably represent the nearest analogues to IMBHs in GCs, and nothing prevents accretion onto the central BH. We have also assumed that the radiative efficiency and accretion rate, parameterized in terms of the Bondi rate, have typical values comparable to nearby low-luminosity accreting central BHs. These observed systems have a large dispersion in the accretion rate and/or efficiency. Some may not have appreciable accretion at all, though others could be accreting at much higher rates or with higher efficiency than assumed. If the dispersion in these quantities is high, then the nondetection of IMBHs in 50 GCs strongly suggests that IMBHs are rare, if they exist at all. We emphasize that the actual accretion rates and radiative efficiencies of IMBHs are the chief uncertainty in this analysis.

Depending on the assumptions for radiative efficiency, our typical VLA limits correspond to very low accretion rates of a few $\times 10^{-11}\ M_{\odot}\ \mathrm{yr}^{-1}$, which is only a few percent of the mass loss rate of one red giant (Dupree et al. 2009). We note that MacLeod et al. (2016) argued that some fraction of GC IMBHs should have nondegenerate companions that could supply a higher rate of gas to the IMBH than accretion from ambient material.

The use of the fundamental plane to convert radio limits to masses is an interpolation between stellar-mass and supermassive BHs rather than an extrapolation. This fact is heartening, but the accretion behavior of hypothetical IMBHs is still unknown. Cseh et al. (2015) found that HLX-1 was more radio bright than predicted by the fundamental plane, assuming that the mass inferred from X-ray spectral fitting was correct. The large (0.4 dex; Plotkin et al. 2012) scatter in the fundamental plane also limits precise statements about accretion implications for specific systems.

5.2. Revisiting IMBHs from the Literature

We begin with ω Cen and M54, as these massive GCs are often argued to be stripped galaxy nuclei (the case for M54 is especially strong; Layden & Sarajedini 2000) and hence may be the most likely to host IMBHs.

5.2.1. ω Cen

ω Cen has many contrasting claims of dynamical evidence for an IMBH (Noyola et al. 2008; Noyola 2010; van der Marel & Anderson 2010; Baumgardt 2017), with some papers finding dynamical evidence for an IMBH with a mass of $\gtrsim 10^4 M_{\odot}$. We do not revisit this work here but focus solely on the accretion constraints. Our 3σ ATCA upper limit of $<8.9\,\mu$Jy on a central radio source implies a 3σ IMBH mass upper limit of $<1000 M_{\odot}$ using our formalism. The corresponding 0.5–10 keV X-ray luminosity limit is $<2.5 \times 10^{30}$ erg s^{-1} (Table 2), which

can be compared to the observed (95%) upper limit of $<1.7 \times 10^{30}$ erg s^{-1} (Haggard et al. 2013). Because of the large amount of *Chandra* data on this cluster, this is one case where the X-ray limit is as (or more) constraining than the radio limit. As discussed in Haggard et al. (2013) and Strader et al. (2012), if an IMBH with a mass of $\gtrsim 10^4 M_\odot$ is present in ω Cen, then it must be accreting at a relative rate below any other central BH known in the universe, with $L_{\rm bol}/L_{\rm edd} \lesssim 2 \times 10^{-11}$. There is no accretion evidence for an IMBH in ω Cen.

5.2.2. M54

In M54, the 3σ radio upper limit of <7.2 μJy gives a mass limit of $<3000 M_\odot$, far below the $9400 M_\odot$ suggested dynamically (Ibata et al. 2009). The new radio limit is about a factor of seven stronger than the one presented in Wrobel et al. (2011), due entirely to the improved sensitivity of the postupgrade VLA. M54 is the nucleus of the Sagittarius dwarf galaxy (e.g., Monaco et al. 2005) with a V band stellar luminosity of $10^8 L_\odot$ and a halo mass of $>6 \times 10^{10} M_\odot$ (Gibbons et al. 2017). While the occupation fraction of BHs is known to be high at the centers of slightly higher-mass galaxies (Nguyen et al. 2017), little is known about the BH occupation fraction at these low masses. Owing to its identity as the closest confirmed galaxy nucleus beyond Sgr A*, in our view M54 presents a strong case for even deeper radio observations.

5.2.3. New Pulsar Evidence: 47 Tuc and NGC 6624

For many years, 47 Tuc was a rare case where most papers agreed that there was no substantial evidence for an IMBH; most prominently, McLaughlin et al. (2006) set a 1σ dynamical upper limit of <1000–1500 $M_\odot$ on an IMBH. This was challenged by Kızıltan et al. (2017), who used the timing of millisecond pulsars in the core of 47 Tuc to argue for the presence of a $2300 M_\odot$ IMBH. Freire et al. (2017) disputed this interpretation of the observations (partially on the basis of the assumed cluster distance) and argued that no IMBH is necessary to explain the pulsar timing data. Our new ATCA 3σ radio upper limit of <11.2 μJy corresponds to a mass limit of $<1040 M_\odot$, suggesting that an IMBH of the mass published by Kızıltan et al. (2017) is not present or that it is accreting at a rate or efficiency lower than assumed in our formalism. 47 Tuc is another cluster, like ω Cen, where there are extremely deep *Chandra* data (Grindlay et al. 2001), which limit a central X-ray source to $<10^{31}$ erg s^{-1} (0.5–10 keV). The corresponding 3σ limit from our formalism is $L_{\rm X} < 2.8 \times 10^{30}$ erg s^{-1}, and a deeper *Chandra* constraint should be possible in the future through the analysis of archival data.

A unique recent claim of dynamical evidence for an IMBH in the GC NGC 6624 comes from Perera et al. (2017), who argued, on the basis of precise long-term timing, that the pulsar PSR 1820-30A is in a wide eccentric orbit around an IMBH. The observational interpretation of this cluster is complicated, and we discuss it in detail in the Appendix. Here we only mention our ATCA radio limit on a central IMBH: a 3σ value of <9.8 μJy, giving a 3σ IMBH mass of <1550 $M_\odot$, compared to a dynamical IMBH mass of 7500–10,000 $M_\odot$ in Perera et al. (2017). With our formalism, the radio flux density of a 7500 $M_\odot$ IMBH would be predicted to be about 700 μJy, which is about a factor of 70 larger than our ATCA limit.

5.2.4. Other Clusters

NGC 6388 is a case similar to ω Cen where there is disagreement in the literature about dynamical evidence for the presence of a (2–3) $\times 10^4 M_\odot$ IMBH (Lützgendorf et al. 2011; Lanzoni et al. 2013; Lützgendorf et al. 2015). Previous ATCA observations gave 3σ upper limits of <81 μJy (at 9 GHz; Cseh et al. 2010) and <42 μJy (at 5.5 GHz; Bozzo et al. 2011). As discussed above, we do observe emission near (but not coincident with) the center of the cluster at 5.5 GHz, which we attribute to unresolved pulsars. Such emission is not unexpected given the strong *Fermi* GeV flux from the cluster. At 9.0 GHz no emission is detected, with a 3σ upper limit of <8.5 μJy, about a factor of five lower than the Bozzo et al. (2011) limit. This corresponds to a 3σ IMBH mass limit of $<1770 M_\odot$, about a factor of 16 lower than the dynamical mass inferred from Lützgendorf et al. (2015).

M15 is a cluster where there were early dynamical hints for an IMBH (Newell 1970; Gerssen et al. 2002, 2003), for which the interpretation was immediately disputed (Illingworth & King 1977; Baumgardt et al. 2003), and subsequent works have generally agreed that no IMBH is required (e.g. den Brok et al. 2014) . Our M15 radio data are the same as presented in Strader et al. (2012), which found no accretion evidence for an IMBH.

There are other clusters for which single studies have suggested dynamical evidence for IMBHs. Lützgendorf et al. (2013a) presented 2σ dynamical evidence for a $\sim 2000 M_\odot$ IMBH in M62, for which our formal VLA 3σ limit is $<1130 M_\odot$. Kamann et al. (2016) suggested that NGC 6397 could host a 600 $M_\odot$ IMBH. This does not conflict with our ATCA limit for this cluster ($<630 M_\odot$). For both of these clusters, Baumgardt (2017) argued that the surface brightness profiles and kinematic data do not require the presence of an IMBH.

5.3. Conclusions and Implications

We have presented the deepest radio observations to date for a sample of 50 Milky Way GCs, with a goal of searching for evidence of central accreting IMBHs. While a few clusters do have radio sources near or in their centers, we do not find any credible IMBH candidates. A stacking analysis of GCs observed with VLA or ATCA also reveals no emission that can be attributed to IMBHs.

We emphasize that for any particular GC it is possible to conceive of mechanisms that would reduce or eliminate the accretion of ambient gas, rendering the IMBH undetectable in current radio or X-ray observations. Yet it is difficult to argue that such conditions should apply in many or most GCs. The most straightforward conclusion to draw from our work is that IMBHs with masses $\gtrsim 10^3 M_\odot$ are either not present or at least not common in GCs.

The recent detections of merging binary BHs through gravitational waves (Abbott et al. 2016) may help explain the observed lack of IMBHs in GCs. If such binary stellar-mass BHs are formed dynamically in GCs (Rodriguez et al. 2016), then it could indicate that single and binary BHs are preferentially ejected from GCs rather than merging with a more massive seed BH to form an IMBH (Miller & Hamilton 2002; Gültekin et al. 2004, 2006; Baker et al. 2008; Moody & Sigurdsson 2009). Of course, there are many ways to grow IMBHs in GCs that do not depend on mergers of smaller BHs (e.g., Portegies Zwart et al. 2004).

We also cannot constrain IMBHs that may have been ejected from GCs (Holley-Bockelmann et al. 2008) or the presence of less massive IMBHs (those of a few hundred $M_{\odot}$) through accretion signatures, especially since such objects may wander far from the cluster center (Lützgendorf et al. 2013b).Theoretical predictions for IMBH masses range widely, from 0.1% to 1% or more of the cluster mass (e.g., Miller & Hamilton 2002; O'Leary et al. 2006; Portegies Zwart et al. 2006; Giersz et al. 2015; Woods et al. 2017). Our median VLA and ATCA limits are in the middle of this range (0.36% and 0.54%), though the extreme values range as low as 0.03% and as high as 2.3%. If IMBHs typically make up only 0.1% of the mass of a GC, then (in the context of our formalism for radio emission) they would be difficult to detect outside the most massive GCs, unless the accretion is more radiatively efficient than we assume. We note that IMBHs well below 1000 $M_{\odot}$ are also not easily detected via standard dynamical techniques (Baumgardt 2017). Future gravitational wave observatories, including eLISA, offer more hope for detecting such IMBHs (Haster et al. 2016)—if they exist.

We thank an anonymous referee and B. Stappers and B. Perera for useful comments. The National Radio Astronomy Observatory is a facility of the National Science Foundation (NSF) operated under cooperative agreement by Associated Universities, Inc. The ATCA is part of the Australia Telescope National Facility, which is funded by the Australian government for operation as a national facility managed by CSIRO.

J.S. acknowledges support from the Packard Foundation. We thank the NSF through support from grants AST-1308124 and AST-1514763. J.C.A.M.-J. is the recipient of an Australian Research Council Future Fellowship (FT140101082). C.O.H. and G.R.S. are supported by NSERC Discovery Grants, and C.O.H. is also supported by an NSERC Discovery Accelerator Supplement. A.C.S. acknowledges financial support from NSF AST-1350389.

Facilities: VLA, ATCA.

Software: CASA (McMullin et al. 2007), AIPS (Wells 1985), TOPCAT (Taylor 2005), APLpy (Robitaille & Bressert 2012), Astropy (Astropy Collaboration et al. 2013).

Appendix

A.1. NGC 6624: The Position of 4U 1820-30

A continuing discussion about the radio continuum imaging of NGC 6624 is whether central radio emission can be attributed to the low-mass X-ray binary 4U 1820-30, the bright pulsar PSR 1820-30A, or a frequency-dependent combination of the two. Owing to the steep spectral slope of the pulsar, it may significantly contribute at low frequencies, but at the higher frequencies of our ATCA observations the contribution of the pulsar is expected to be minimal (Migliari et al. 2004). One issue with this argument in the past has been that the location of the radio emission was not entirely consistent with that of 4U 1820-30, independently determined via *HST* imaging of the UV-bright optical counterpart to the X-ray binary.

We first revisit the position of the optical counterpart to 4U 1820-30 using new *HST* data taken with WFC3 (Program GO-13297; P.I. Piotto). 4U 1820-30 is the brightest source in the core of the cluster in *F*275W; however, many of the *Gaia* stars in the initial DR1 data release in the field of view of this image are not well detected. Hence we instead focus on *F*336W, in which 4U 1820-30 is still bright but the number of well-detected *Gaia* stars is larger. We correct the astrometry of the *F*336W *HST* image using the *Gaia* stars, achieving a solution with an rms uncertainty of 13–14 mas per coordinate. The J2000 position of this star is (R.A., decl.) = (18:23:40.4975 ± 0.0010s, –30:21:40.096 ± 0.″017).

To determine the position of the radio source in our ATCA images we use the 9.0 GHz image, which has the best resolution, finding a J2000 position of (R.A., decl.) = (18:23:40.4978 ± 0.0005s, –30:21:40.081 ± 0.″024). The difference between our ATCA 9.0 GHz position and the *HST* *F*336W position is 0.″016—the two positions agree even within their small uncertainties. Hence we conclude that the radio emission at 9.0 GHz is entirely due to 4U 1820-30 and that the position of this binary is well determined. 4U 1820-30 is located 0.″43 from the cluster center.

We next compare this position to that found in previous work. It is just outside of the larger error circle of the VLA source found by Migliari et al. (2004) at 4.9 and 8.4 GHz—consistent at the 1.3σ level. However, it is entirely inconsistent with the previous *HST* position by Sosin & King (1995), differing by 0.″58. This has important implications for the interpretation of the properties of 4U 1820-30: rather than being more distant from the cluster center than PSR 1820-30A, it is at a similar distance.

We note that our new position for 4U 1820-30 differs from the ALMA position found by Díaz Trigo et al. (2017) by 0.″36; this difference is nominally highly significant given the stated positional uncertainties. However, both positions are approximately the same distance from the cluster center (about 0.″4 in both cases), so they do not change the interpretation of the X-ray binary properties in the context of an IMBH. Understanding the source of this discrepancy is beyond the scope of the current paper.

A.2. Implications

Perera et al. (2017) studied long-term radio timing observations of PSR 1820-30A, located close to the center of NGC 6624. These observations admit two possibilities: that PSR 1820-30A is in an extremely wide, eccentric orbit around a massive IMBH, or that it is in a less-eccentric orbit with a normal star or stellar remnant. One of their arguments in favor of the IMBH interpretation is that the unexpected negative orbital period derivative of 4U 1820-30 is due to an acceleration that requires the addition of an IMBH to the cluster potential.

From reviewing the literature it is clear that a series of errors has propagated since the earliest identification of 4U 1820-30 with *HST*. The first paper to locate the source was King et al. (1993), who found that 4U 1820-30 was located 0.″66 N of the cluster center (from their abstract; the listed positions actually imply only 0.″6, possibly due to rounding). Sosin & King (1995) "corrected" a 1.″8 error in the absolute astrometry of King et al. (1993) and refined the cluster center, but the relative distance of 4U 1820-30 from the center was essentially unchanged at 0.″67.

Peuten et al. (2014) reported that if the updated Goldsbury et al. (2010) center is used, then 4U 1820-30 is 0.046 pc from the cluster center (1.″2 at Peuten et al. 2014's assumed distance of 7.9 kpc). We are unable to determine the origin of this value. The distance of the King et al. (1993) position from the Goldsbury et al. (2010) center is 0.″98; if the X-ray binary

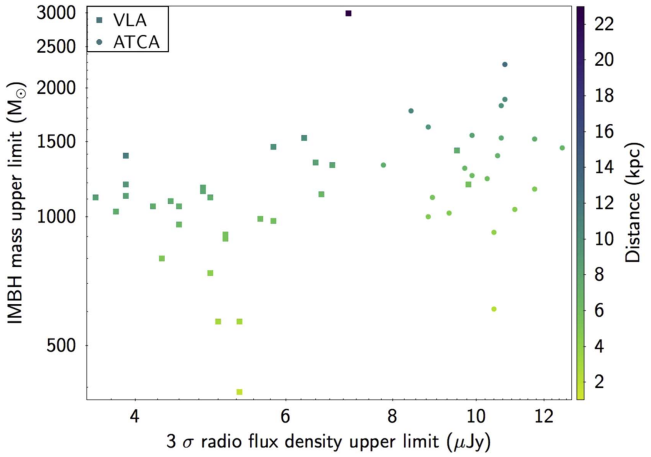

Figure 7. IMBH mass upper limits as a function of radio flux density upper limits for VLA (squares) and ATCA (circles). The colors of symbols denote distance, as shown in the color-bar at right. Both axes are plotted in logarithmic scales. M4 shows the lowest IMBH mass upper limit while the next-lowest IMBH upper limits from the VLA are for NGC 6544 and M22. From ATCA data, NGC 6397 has the lowest IMBH mass upper limit.

position from Sosin & King (1995) is used, then the distance from the new center is 0.″83.

Perera et al. (2017) cited Migliari et al. (2004) for the position of 4U 1820-30, who in turn took the position from Sosin & King (1995). However, the value published by Migliari et al. (2004) is rounded off, and hence the separation of 4U 1820-30 from the center implied is slightly larger than the correct value (0.″87 instead of 0.″83). Notwithstanding this rounding, the positions in their Table 1 and Figure 1 are accurately rendered and would imply a separation of 0.032 pc (for 7.9 kpc). However, in their Figure 9 that summarizes the dynamical constraints, and in their Erratum Figure 1, the separation plotted for 4U 1820-30 is simply the physical value from Peuten et al. (2014), 0.046 pc. The incorrect separation from Peuten et al. (2014) is repeated in Gieles et al. (2018), who argued, contra Perera et al. (2017), that in any case most or all of the period change can be attributed to intrinsic factors.

The propagation of this mistake through the literature caused an overinterpretation of the 4U 1820-30 period derivative when only considering the information available. Our new *HST* position doubles down: we find that 4U 1820-30 is $0.43 \pm 0.''10$ from the Goldsbury et al. (2010) center. This is equivalent to 0.0175 ± 0.0041 pc using our assumed distance of 8.4 kpc (using 7.9 kpc instead would not change any of the conclusions). This is nearly identical to the separation between PSR 1820-30A and the center using the updated position of the pulsar from Perera et al. (2017); given the uncertainties in the center, either source may actually be closer. We do not present updated dynamical models of NGC 6624 in this paper, but only note that using the correct position of 4U 1820-30 would lower the inferred IMBH mass—if its period derivative is interpreted as being dominated by the potential of an IMBH, rather than intrinsic factors.

A.3. The Radio Properties of 4U 1820-30

Considering the radio properties of 4U 1820-30 itself: the flux density of 4U 1820-30 is $235 \pm 4\,\mu$Jy (5.5 GHz) and $207 \pm 4\ \mu$Jy (9.0 GHz), yielding a spectral index of $\alpha = -0.26 \pm 0.06$ for a power-law $S_\nu \propto \nu^\alpha$. Previous radio continuum observations at similar frequencies have been made with the VLA (mean flux densities of 130 ± 40 and $100 \pm 20\,\mu$Jy at 4.9 and 8.4 GHz, respectively; Migliari et al. 2004) and with ATCA (flux densities of 236 ± 27 and $<200\,\mu$Jy at 5.5 and 9.0 GHz; Díaz Trigo et al. 2017). Our new flux densities are a factor of $\sim$2 higher than those measured with the old VLA, possibly related to the well-known superorbital modulation in X-rays (Chou & Grindlay 2001). Our 5.5 GHz ATCA measurement is spot on with the 2014 ATCA measurement made simultaneously with ALMA observations (Díaz Trigo et al. 2017). Our 9.0 GHz measurement is nominally inconsistent with the upper limit of $<200\,\mu$Jy reported by Díaz Trigo et al. (2017), but only marginally so. In any case, the flux density of 4U 1820-30 and its spectral slope are extremely well measured in these new observations.

Given that we find a flux density at 5.5 GHz identical to Díaz Trigo et al. (2017), it seems reasonable to combine their 302 GHz ALMA flux density of $400 \pm 20\,\mu$Jy with our ATCA measurements at 5.5 and 9.0 GHz to determine the radio/mm spectral energy distribution of the binary. In this case, we find that the 5.5, 9.0 and 302 GHz flux densities are strongly inconsistent with a single power law. This suggests either that the ALMA observations (taken 1 week from the 2014 ATCA data) were taken during a flare unobserved at other wavelengths or that there is another source of 302 GHz emission. Truly simultaneous radio and mm observations of 4U 1820-30 appear necessary to determine an accurate spectral energy distribution for this binary.

ORCID iDs

Evangelia Tremou https://orcid.org/0000-0002-4039-6703
Jay Strader https://orcid.org/0000-0002-1468-9668
Laura Chomiuk https://orcid.org/0000-0002-8400-3705
James C. A. Miller-Jones https://orcid.org/0000-0003-3124-2814
Craig O. Heinke https://orcid.org/0000-0003-3944-6109
Gregory R. Sivakoff https://orcid.org/0000-0001-6682-916X

References

Abbott, B. P., Abbott, R., Abbott, T. D., et al. 2016, PhRvL, 116, 061102
Abdo, A. A., Ackermann, M., Ajello, M., et al. 2010, A&A, 524, A75
Anderson, J., & van der Marel, R. P. 2010, ApJ, 710, 1032
Arellano Ferro, A., Bramich, D. M., Figuera Jaimes, R., et al. 2013, MNRAS, 434, 1220
Astropy Collaboration, Robitaille, T. P., Tollerud, E. J., et al. 2013, A&A, 558, A33
Bahramian, A., Heinke, C. O., Sivakoff, G. R., & Gladstone, J. C. 2013, ApJ, 766, 136
Baker, J. G., Boggs, W. D., Centrella, J., et al. 2008, ApJL, 682, L29
Baldassare, V. F., Reines, A. E., Gallo, E., & Greene, J. E. 2015, ApJL, 809, L14
Baumgardt, H. 2017, MNRAS, 464, 2174
Baumgardt, H., & Hilker, M. 2018, MNRAS, 478, 1520
Baumgardt, H., Hut, P., Makino, J., McMillan, S., & Portegies Zwart, S. 2003, ApJL, 582, L21
Baumgardt, H., Makino, J., & Hut, P. 2005, ApJ, 620, 238
Blandford, R. D., & Königl, A. 1979, ApJ, 232, 34
Bogdanov, S., Heinke, C. O., Özel, F., & Güver, T. 2016, ApJ, 831, 184
Bondi, H. 1952, MNRAS, 112, 195
Bozzo, E., Ferrigno, C., Stevens, J., et al. 2011, A&A, 535, L1
Bromm, V., & Loeb, A. 2003, ApJ, 596, 34
Cackett, E. M., Wijnands, R., Heinke, C. O., et al. 2006, MNRAS, 369, 407
Cadelano, M., Ransom, S. M., Freire, P. C. C., et al. 2018, ApJ, 855, 125
Chatterjee, P., Hernquist, L., & Loeb, A. 2002, ApJ, 572, 371

Chou, Y., & Grindlay, J. E. 2001, ApJ, 563, 934
Cohen, J. G., Hsieh, S., Metchev, S., Djorgovski, S. G., & Malkan, M. 2007, AJ, 133, 99
Cohen, R. E., Mauro, F., Geisler, D., et al. 2014, AJ, 148, 18
Contreras, R., Catelan, M., Smith, H. A., et al. 2010, AJ, 140, 1766
Cseh, D., Kaaret, P., Corbel, S., et al. 2010, MNRAS, 406, 1049
Cseh, D., Webb, N. A., Godet, O., et al. 2015, MNRAS, 446, 3268
Dalessandro, E., Beccari, G., Lanzoni, B., et al. 2009, ApJS, 182, 509
Dalessandro, E., Lanzoni, B., Beccari, G., et al. 2011, ApJ, 743, 11
D'Amico, N., Lyne, A. G., Manchester, R. N., Possenti, A., & Camilo, F. 2001, ApJL, 548, L171
de Vita, R., Trenti, M., & MacLeod, M. 2018, MNRAS, 475, 1574
DeCesar, M. E., Ransom, S. M., Kaplan, D. L., Ray, P. S., & Geller, A. M. 2015, ApJL, 807, L23
den Brok, M., van de Ven, G., van den Bosch, R., & Watkins, L. 2014, MNRAS, 438, 487
Díaz Trigo, M., Migliari, S., Miller-Jones, J. C. A., et al. 2017, A&A, 600, A8
Djorgovski, S. 1987, ApJL, 317, L13
Dupree, A. K., Smith, G. H., & Strader, J. 2009, AJ, 138, 1485
Eisenstein, D. J., & Loeb, A. 1995, ApJ, 443, 11
Falcke, H., Körding, E., & Markoff, S. 2004, A&A, 414, 895
Fall, S. M., & Rees, M. J. 1985, ApJ, 298, 18
Farrell, S. A., Servillat, M., Gladstone, J. C., et al. 2014, MNRAS, 437, 1208
Feldmeier, A., Lützgendorf, N., Neumayer, N., et al. 2013, A&A, 554, A63
Feng, H., & Soria, R. 2011, NewAR, 55, 166
Ferrara, A., Haardt, F., & Salvaterra, R. 2013, MNRAS, 434, 2600
Ferraro, F. R., Messineo, M., Fusi Pecci, F., et al. 1999, AJ, 118, 1738
Fregeau, J. M., Joshi, K. J., Portegies Zwart, S. F., et al. 2002, ApJ, 570, 171
Freire, P. C., Kramer, M., Lyne, A. G., et al. 2001, ApJL, 557, L105
Freire, P. C. C., Ridolfi, A., Kramer, M., et al. 2017, MNRAS, 471, 857
Fruchter, A. S., & Goss, W. M. 2000, ApJ, 536, 865
Gallo, E., Fender, R. P., & Hynes, R. I. 2005, MNRAS, 356, 1017
Gebhardt, K., Rich, R. M., & Ho, L. C. 2005, ApJ, 634, 1093
Gerssen, J., van der Marel, R. P., Gebhardt, K., et al. 2002, AJ, 124, 3270
Gerssen, J., van der Marel, R. P., Gebhardt, K., et al. 2003, AJ, 125, 376
Gibbons, S. L. J., Belokurov, V., & Evans, N. W. 2017, MNRAS, 464, 794
Gieles, M., Balbinot, E., Yaaqib, R. I. S. M., et al. 2018, MNRAS, 473, 4832
Giersz, M., Leigh, N., Hypki, A., et al. 2015, MNRAS, 454, 3150
Goldsbury, R., Richer, H. B., Anderson, J., et al. 2010, AJ, 140, 1830
Greisen, E. W. 2003, ASSL, 285, 109
Grindlay, J. E., Heinke, C., Edmonds, P. D., et al. 2001, Sci, 292, 2290
Gültekin, K., Miller, M. C., & Hamilton, D. P. 2004, ApJ, 616, 221
Gültekin, K., Miller, M. C., & Hamilton, D. P. 2006, ApJ, 640, 156
Gürkan, M. A., Freitag, M., & Rasio, F. A. 2004, ApJ, 604, 632
Haggard, D., Cool, A. M., Heinke, C. O., et al. 2013, ApJL, 773, L31
Harris, W. E. 1996, AJ, 112, 1487
Harris, W. E. 2010, arXiv:1012.3224
Haster, C.-J., Antonini, F., Kalogera, V., & Mandel, I. 2016, ApJ, 832, 192
Hjellming, R. M., & Johnston, K. J. 1988, ApJ, 328, 600
Holley-Bockelmann, K., Gültekin, K., Shoemaker, D., & Yunes, N. 2008, ApJ, 686, 829
Ibata, R., Bellazzini, M., Chapman, S. C., et al. 2009, ApJL, 699, L169
Illingworth, G., & King, I. R. 1977, ApJL, 218, L109
in't Zand, J. J. M., Hulleman, F., Markwardt, C. B., et al. 2003, A&A, 406, 233
Inayoshi, K., Ostriker, J. P., Haiman, Z., & Kuiper, R. 2018, MNRAS, 476, 1412
Johnston, H. M., Kulkarni, S. R., & Goss, W. M. 1991, ApJL, 382, L89
Kaluzny, J., Thompson, I. B., Rozyczka, M., & Krzeminski, W. 2013, AcA, 63, 181
Kamann, S., Husser, T.-O., Brinchmann, J., et al. 2016, A&A, 588, A149
Kamann, S., Wisotzki, L., Roth, M. M., et al. 2014, A&A, 566, A58
King, I. R., Stanford, S. A., Albrecht, R., et al. 1993, ApJL, 413, L117
Kızıltan, B., Baumgardt, H., & Loeb, A. 2017, Natur, 542, 203
Kunder, A., Stetson, P. B., Cassisi, S., et al. 2013, AJ, 146, 119
Lanzoni, B., Ferraro, F. R., Dalessandro, E., et al. 2010, ApJ, 717, 653
Lanzoni, B., Mucciarelli, A., Origlia, L., et al. 2013, ApJ, 769, 107
Layden, A. C., & Sarajedini, A. 2000, AJ, 119, 1760
Lindroos, L., Knudsen, K. K., Vlemmings, W., Conway, J., & Martí-Vidal, I. 2015, MNRAS, 446, 3502
Lodato, G., & Natarajan, P. 2006, MNRAS, 371, 1813
Loeb, A., & Rasio, F. A. 1994, ApJ, 432, 52
Lu, T.-N., & Kong, A. K. H. 2011, ApJL, 729, L25
Lützgendorf, N., Gebhardt, K., Baumgardt, H., et al. 2015, A&A, 581, A1
Lützgendorf, N., Kissler-Patig, M., Gebhardt, K., et al. 2013a, A&A, 552, A49
Lützgendorf, N., Kissler-Patig, M., Neumayer, N., et al. 2013b, A&A, 555, A26
Lützgendorf, N., Kissler-Patig, M., Noyola, E., et al. 2011, A&A, 533, A36
Lynch, R. S., Freire, P. C. C., Ransom, S. M., & Jacoby, B. A. 2012, ApJ, 745, 109
Maccarone, T. J. 2003, A&A, 409, 697
Maccarone, T. J. 2004, MNRAS, 351, 1049
Maccarone, T. J., Fender, R. P., & Tzioumis, A. K. 2005, Ap&SS, 300, 239
Maccarone, T. J., & Servillat, M. 2008, MNRAS, 389, 379
MacLeod, M., Trenti, M., & Ramirez-Ruiz, E. 2016, ApJ, 819, 70
Madau, P., & Rees, M. J. 2001, ApJL, 551, L27
Matsubayashi, T., Makino, J., & Ebisuzaki, T. 2007, ApJ, 656, 879
Maxwell, J. E., Lugger, P. M., Cohn, H. N., et al. 2012, ApJ, 756, 147
McLaughlin, D. E., Anderson, J., Meylan, G., et al. 2006, ApJS, 166, 249
McMullin, J. P., Waters, B., Schiebel, D., Young, W., & Golap, K. 2007, in ASP Conf. Ser. 376, adass XVI, ed. R. A. Shaw, F. Hill, & D. J. Bell (San Francisco, CA: ASP), 127
Merloni, A., Heinz, S., & di Matteo, T. 2003, MNRAS, 345, 1057
Migliari, S., Fender, R. P., Rupen, M., et al. 2004, MNRAS, 351, 186
Miller, M. C., & Hamilton, D. P. 2002, MNRAS, 330, 232
Miller-Jones, J. C. A., Sivakoff, G. R., Heinke, C. O., et al. 2011, ATel, 3378
Miller-Jones, J. C. A., Wrobel, J. M., Sivakoff, G. R., et al. 2012, ApJL, 755, L1
Miocchi, P., Lanzoni, B., Ferraro, F. R., et al. 2013, ApJ, 774, 151
Monaco, L., Bellazzini, M., Ferraro, F. R., & Pancino, E. 2005, MNRAS, 356, 1396
Moody, K., & Sigurdsson, S. 2009, ApJ, 690, 1370
Musaeva, A., Koribalski, B. S., Farrell, S. A., et al. 2015, MNRAS, 447, 1951
Nagar, N. M., Falcke, H., Wilson, A. S., et al. 2000, ApJ, 542, 186
Naiman, J., Soares-Furtado, M., & Ramirez-Ruiz, E. 2013, ApJ, submitted (arXiv:1310.8301)
Narayan, R., & Yi, I. 1995, ApJ, 452, 710
Newell, B., da Costa, G. S., & Norris, J. 1976, ApJL, 208, L55
Newell, E. B. 1970, ApJ, 159, 443
Nguyen, D. D., Seth, A. C., den Brok, M., et al. 2017, ApJ, 836, 237
Noyola, E. 2010, BAAS, 42, 445
Noyola, E., & Baumgardt, H. 2011, ApJ, 743, 52
Noyola, E., & Gebhardt, K. 2006, AJ, 132, 447
Noyola, E., Gebhardt, K., & Bergmann, M. 2008, ApJ, 676, 1008
Nyland, K., Davis, T. A., Nguyen, D. D., et al. 2017, ApJ, 845, 50
O'Leary, R. M., Rasio, F. A., Fregeau, J. M., et al. 2006, ApJ, 637, 937
Ortolani, S., Barbuy, B., Bica, E., et al. 1999, A&A, 350, 840
Ortolani, S., Barbuy, B., Bica, E., Zoccali, M., & Renzini, A. 2007, A&A, 470, 1043
Ortolani, S., Bica, E., & Barbuy, B. 2003, A&A, 402, 565
Paltrinieri, B., Ferraro, F. R., Paresce, F., & de Marchi, G. 2001, AJ, 121, 3114
Pavlinsky, M. N., Grebenev, S. A., & Sunyaev, R. A. 1994, ApJ, 425, 110
Pellegrini, S. 2005, ApJ, 624, 155
Perera, B. B. P., Stappers, B. W., Lyne, A. G., et al. 2017, MNRAS, 468, 2114
Peuten, M., Brockamp, M., Küpper, A. H. W., & Kroupa, P. 2014, ApJ, 795, 116
Pfahl, E., & Rappaport, S. 2001, ApJ, 550, 172
Picard, A., & Johnston, H. M. 1995, A&AS, 112, 89
Plotkin, R. M., Markoff, S., Kelly, B. C., Körding, E., & Anderson, S. F. 2012, MNRAS, 419, 267
Pooley, D., & Rappaport, S. 2006, ApJL, 644, L45
Portegies Zwart, S. F., Baumgardt, H., McMillan, S. L. W., et al. 2006, ApJ, 641, 319
Portegies Zwart, S. F., Dewi, J., & Maccarone, T. 2004, MNRAS, 355, 413
Portegies Zwart, S. F., & McMillan, S. L. W. 2002, ApJ, 576, 899
Possenti, A., D'Amico, N., Manchester, R. N., et al. 2003, ApJ, 599, 475
Prager, B. J., Ransom, S. M., Freire, P. C. C., et al. 2017, ApJ, 845, 148
Predehl, P., Hasinger, G., & Verbunt, F. 1991, A&A, 246, L21
Ransom, S. M., Hessels, J. W. T., Stairs, I. H., et al. 2005, Sci, 307, 892
Rau, U. 2012, Proc. SPIE, 8500, 85000N
Robitaille, T., & Bressert, E. 2012, APLpy: Astronomical Plotting Library in Python, Astrophysics Source Code Library, ascl:1208.017
Rodriguez, C. L., Chatterjee, S., & Rasio, F. A. 2016, PhRvD, 93, 084029
Saracino, S., Dalessandro, E., Ferraro, F. R., et al. 2015, ApJ, 806, 152
Sault, R. J., Teuben, P. J., & Wright, M. C. H. 1995, in Proc. ASP Conf. Ser 77, adass IV, ed. R. A. Shaw, H. E. Payne, & J. J. E. Hayes (San Francisco, CA: ASP), 433
Shawl, S. J., & White, R. E. 1986, AJ, 91, 312
Soria, R., Musaeva, A., Wu, K., et al. 2017, MNRAS, 469, 886
Sosin, C., & King, I. R. 1995, AJ, 109, 639
Spergel, D. N. 1991, Natur, 352, 221
Stacey, W. S., Heinke, C. O., Cohn, H. N., Lugger, P. M., & Bahramian, A. 2012, ApJ, 751, 62
Strader, J., Chomiuk, L., Maccarone, T. J., et al. 2012, ApJL, 750, L27
Taylor, M. B. 2005, adass XIV, 347, 29

Trager, S. C., King, I. R., & Djorgovski, S. 1995, AJ, 109, 218
Trenti, M. 2006, arXiv:astro-ph/0612040
Valenti, E., Ferraro, F. R., & Origlia, L. 2007, AJ, 133, 1287
Valenti, E., Ferraro, F. R., & Origlia, L. 2010, MNRAS, 402, 1729
Valenti, E., Origlia, L., & Ferraro, F. R. 2005, MNRAS, 361, 272
van der Marel, R. P., & Anderson, J. 2010, ApJ, 710, 1063
van Loon, J. T., Stanimirović, S., Evans, A., & Muller, E. 2006, MNRAS, 365, 1277
Vanbeveren, D., Belkus, H., van Bever, J., & Mennekens, N. 2009, Ap&SS, 324, 271
Vanderbeke, J., de Propris, R., de Rijcke, S., et al. 2015, MNRAS, 450, 2692
Vesperini, E., McMillan, S. L. W., D'Ercole, A., & D'Antona, F. 2010, ApJL, 713, L41
Volonteri, M., & Perna, R. 2005, MNRAS, 358, 913
Watkins, L. L., van der Marel, R. P., Bellini, A., et al. 2016, MmSAI, 87, 610
Watkins, L. L., van der Marel, R. P., Bellini, A., & Anderson, J. 2015, ApJ, 812, 149
Webb, N., Cseh, D., Lenc, E., et al. 2012, Sci, 337, 554
Webb, N. A., Guérou, A., Ciambur, B., et al. 2017, A&A, 602, A103
Wells, D. C. 1985, in Data Analysis in Astronomy, ed. V. Di Gesù et al. (New York: Plenum Press), 195
Wilson, W. E., Ferris, R. H., Axtens, P., et al. 2011, MNRAS, 416, 832
Wolszczan, A., Kulkarni, S. R., Middleditch, J., et al. 1989, Natur, 337, 531
Woods, T. E., Heger, A., Whalen, D. J., et al. 2017, ApJL, 842, L6
Wrobel, J. M., Greene, J. E., & Ho, L. C. 2011, AJ, 142, 113
Wrobel, J. M., Miller-Jones, J. C. A., & Middleton, M. J. 2016, AJ, 152, 22
Wrobel, J. M., Nyland, K. E., & Miller-Jones, J. C. A. 2015, AJ, 150, 120
Zinn, R., & Barnes, S. 1998, AJ, 116, 1736